THE JOURNAL OF BIOLOGICAL CHEMISTRY VOL. 289, NO. 48, pp. 33568–33589, November 28, 2014

The Anticancer Agent Di-2-pyridylketone 4,4-Dimethyl-3-thiosemicarbazone (Dp44mT) Overcomes Prosurvival Autophagy by Two Mechanisms

PERSISTENT INDUCTION OF AUTOPHAGOSOME SYNTHESIS AND IMPAIRMENT OF LYSOSOMAL INTEGRITY

Received for publication, July 25, 2014, and in revised form, October 8, 2014 Published, JBC Papers in Press, October 9, 2014, DOI 10.1074/jbc.M114.599480

Elaine Gutierrez[1], **Des R. Richardson**[2,3], **and Patric J. Jansson**[2,4]

From the Molecular Pharmacology and Pathology Program, Department of Pathology and Bosch Institute, Blackburn Building (D06), University of Sydney, Sydney, New South Wales 2006, Australia

Background: Autophagy is a prosurvival mechanism contributing to resistance against anticancer agents.
Results: We demonstrate that the selective antitumor thiosemicarbazone di-2-pyridylketone 4,4-dimethyl-3-thiosemicarbazone (Dp44mT) increases autophagosome synthesis but induces cell death by reducing autophagosome degradation.
Conclusion: Dp44mT overcomes autophagy and utilizes the autophagic machinery to provoke cell death.
Significance: These results indicate a new mechanism by which Dp44mT induces tumor cell death.

Autophagy functions as a survival mechanism during cellular stress and contributes to resistance against anticancer agents. The selective antitumor and antimetastatic chelator di-2-pyridylketone 4,4-dimethyl-3-thiosemicarbazone (Dp44mT) causes lysosomal membrane permeabilization and cell death. Considering the integral role of lysosomes in autophagy and cell death, it was important to assess the effect of Dp44mT on autophagy to further understand its mechanism of action. Notably, Dp44mT affected autophagy by two mechanisms. First, concurrent with its antiproliferative activity, Dp44mT increased the expression of the classical autophagic marker LC3-II as a result of induced autophagosome synthesis. Second, this effect was supplemented by a reduction in autophagosome degradation as shown by the accumulation of the autophagic substrate and receptor p62. Conversely, the classical iron chelator desferrioxamine induced autophagosome accumulation only by inhibiting autophagosome degradation. The formation of redox-active iron or copper Dp44mT complexes was critical for its dual effect on autophagy. The cytoprotective antioxidant *N*-acetylcysteine inhibited Dp44mT-induced autophagosome synthesis and p62 accumulation. Importantly, Dp44mT inhibited autophagosome degradation via lysosomal disruption. This effect prevented the fusion of lysosomes with autophagosomes to form autolysosomes, which is crucial for the completion of the autophagic process. The antiproliferative activity of Dp44mT was suppressed by Beclin1 and ATG5 silencing, indicating the role of persistent autophagosome synthesis in Dp44mT-induced cell death. These studies demonstrate that Dp44mT can overcome the prosurvival activity of autophagy in cancer cells by utilizing this process to potentiate cell death.

Autophagy is a prosurvival, catabolic process involving lysosomal degradation and recycling of long lived proteins and organelles (1). Execution of autophagy begins with the interplay of proteins such as the class III phosphoinositide 3-kinase (PI3K)·Beclin1 complex, ATG5·ATG12, and microtubule-associated protein 1 light chain 3 (LC3)[5]-phosphatidylethanolamine conjugation system that results in the formation of a double membrane vesicle called the autophagosome (1). Proteins and/or organelles are then selectively targeted and shuttled into the autophagosome by receptor proteins such as p62 (1, 2). Finally, the mature autophagosome fuses with the lysosome to form the autolysosome in which the contents are degraded by lysosomal hydrolases (3).

Autophagy protects cells against damaged and harmful components and maintains nutrient and energy homeostasis via the recycling of amino acids, sugars, and metal ions (3–5). For this reason, a considerable proportion of cellular labile iron, generated from the degradation of iron-containing metalloproteins (*e.g.* ferritin), is thought to be present in autolysosomes (6–8).

Considering that rapidly growing neoplastic cells have a higher iron and copper requirement than their normal counterparts, sequestration of metal ions using iron chelators has been shown to be an effective antitumor strategy (9–12). Desferrioxamine (DFO) is a well known iron chelator clinically

[1] Supported by an Australian Postgraduate Award from the University of Sydney.
[2] Both authors contributed equally to this work as senior and corresponding authors.
[3] Supported by a National Health and Medical Research Council of Australia Senior Principal Research Fellowship and Project Grant funding. To whom correspondence may be addressed. Tel.: 61-2-9036-6548; Fax: 61-2-9036-6549; E-mail: d.richardson@sydney.edu.au.
[4] Supported by a Cancer Institute of New South Wales Early Career Research Fellowship. To whom correspondence may be addressed. Tel.: 61-2-9036-7120; Fax: 61-2-9351-3429; E-mail: patric.jansson@sydney.edu.au.

[5] The abbreviations used are: LC3, microtubule-associated protein 1 light chain 3; Act D, actinomycin D; Baf A1, bafilomycin A1; Cat D, cathepsin D; DFO, desferrioxamine; Dp2mT, di-2-pyridylketone 2-methyl-3-thiosemicarbazone; Dp44mT, di-2-pyridylketone 4,4-dimethyl-3-thiosemicarbazone; LAMP-2, lysosome-associated membrane protein 2; LMP, lysosomal membrane permeabilization; NAC, *N*-acetylcysteine; ROS, reactive oxygen species; TAM, tamoxifen; MTT, 3-(4,5-dimethylthiazol-2-yl)-2,5-diphenyltetrazolium bromide.

used for the treatment of iron overload disease (*e.g.* β-thalassemia) and has shown mild antiproliferative activity against cancer cells *in vitro*, in tumors in animal models, and in clinical trials in humans (9, 12–16). However, DFO was demonstrated to have limited efficacy due to its low lipophilicity and membrane permeability (9, 17–19).

Recently, the lipophilic ligand di-2-pyridylketone 4,4-dimethyl-3-thiosemicarbazone (Dp44mT) showed pronounced and selective antitumor and antimetastatic activity *in vitro* and *in vivo* (20–24). Unlike DFO, Dp44mT forms redox-active iron or copper complexes that play key roles in its cytotoxic activity (20, 25–28). In fact, Dp44mT was shown to be lysosomotropic and was retained within lysosomes due to their acidic pH and the ionization characteristics of Dp44mT (27). Within this organelle, Dp44mT forms cytotoxic iron or copper complexes that generate reactive oxygen species (ROS) that result in lysosomal membrane permeabilization and cell death (27).

Given that Dp44mT and DFO both localize to the lysosomal compartment and bind iron or copper (27, 29), the effect of Dp44mT and DFO on autophagy is of interest. Because DFO is known to induce cell death (30) and Dp44mT is potently cytotoxic (20), it is of interest whether autophagy will play a prosurvival role (1, 4). In general, the up-regulation of autophagy results in resistance against anticancer agents by allowing residual or metastasized tumor cells to tolerate cytotoxic stress (1, 4). Thus, inhibition of autophagy in resistant tumors can cause cancer cell death (4). In fact, targeted knockdown of genes essential for autophagy such as *ATG5* and *BECN1* or using autophagy inhibitors such as chloroquine, bafilomycin A1, etc. has led to the resensitization of resistant tumor cells to anticancer therapy (31–34). In contrast, previous studies have also reported a prodeath function of persistent autophagy where blocking the autophagic response using the inhibitor 3-methyladenine or the silencing of autophagy genes *ATG5*, *ATG7*, and *BECN1* inhibited cell death (35, 36). Furthermore, in response to various agents, apoptosis-resistant fibroblasts undergo cell death associated with autophagosome/autolysosome accumulation (37, 38). These findings indicate the role of autophagic cell death as an alternative death mechanism to apoptosis (37, 38).

In this investigation, we demonstrated that Dp44mT regulates autophagy by two mechanisms: 1) increasing autophagosome formation and 2) preventing autophagosome turnover. This latter effect was due to the lysosomal disruption mediated by the formation of copper and iron complexes of Dp44mT. Subsequently, this lysosomal disruption prevented the fusion of the lysosome with the autophagosome, inhibiting the development of functional autolysosomes. Significantly, studies inhibiting the initiation of autophagy using either *BECN1* or *ATG5* silencing suppressed the antiproliferative activity of Dp44mT, demonstrating the role of persistent autophagosome synthesis in Dp44mT-induced cell death. We show that Dp44mT overcame the prosurvival activity of autophagy and converted it into a mechanism of cytotoxicity.

MATERIALS AND METHODS

Cell Culture and Reagents—Human MCF7, MDA-MB-231, and T47D breast cancer cells used in this study were obtained from the American Type Culture Collection (ATCC, Manassas, VA). These cell lines were maintained at 37 °C in a humidified atmosphere of 5% CO_2 in minimum essential medium supplemented with 10% (v/v) fetal bovine serum (FBS), 1% (v/v) nonessential amino acids, 1% (v/v) sodium pyruvate, 2 mM L-glutamine, 100 units/ml penicillin, and 100 μg/ml streptomycin (Invitrogen). Both Dp44mT and di-2-pyridylketone 2-methyl-3-thiosemicarbazone (Dp2mT) were synthesized and characterized using standard procedures (39, 40). DFO was purchased from Novartis (Basel, Switzerland). Tamoxifen, bafilomycin A1, actinomycin D, and *N*-acetylcysteine were obtained from Sigma-Aldrich.

3-(4,5-Dimethylthiazol-2-yl)-2,5-diphenyltetrazolium Bromide (MTT) Cell Viability Assay—Cell viability was examined using the MTT (Sigma-Aldrich) assay by established methods in our laboratory (41). Results were validated by comparison with direct cell counts using trypan blue (41).

Western Blot Analysis—Protein extraction and Western blotting were performed using standard methods (42). Immunodetection of proteins was accomplished using antibodies against LC3 (catalog number MBPM036, Abacus-ALS, Brisbane, Australia), p62 (catalog number ab56416, Abcam, Cambridge, UK), ATG5 (catalog number 2630S, Cell Signaling Technology, Beverly, MA), Beclin1 (catalog number 3738S, Cell Signaling Technology), Bax (catalog number 2772S, Cell Signaling Technology), Bcl-2 (catalog number 2876S, Cell Signaling Technology), and β-actin (catalog number A1978, Sigma-Aldrich). The secondary antibodies implemented include horseradish peroxidase (HRP)-conjugated anti-rabbit (catalog number A6154) and anti-mouse (catalog number A4416) antibodies from Sigma-Aldrich. The membrane was developed using enhanced chemiluminescence (ECL) and imaged using a ChemiDoc (Bio-Rad) imager. Densitometric analysis was performed to quantify the intensities of each band produced using Image Lab Software (Bio-Rad). The relative intensities of target protein bands were normalized to β-actin.

RNA Isolation and Semiquantitative Reverse Transcription (RT)-PCR—Total RNA was isolated by established methods (43) using TRIzol® (Sigma Aldrich). Semiquantitative RT-PCR was performed (43) using the primers in Table 1. β-Actin was used as an RNA loading control. RT-PCR was shown to be semiquantitative and in the log phase of amplification. All RT-PCR products were analyzed by agarose gel electrophoresis. Images were taken utilizing a Gel-Doc (Bio-Rad) apparatus.

Immunofluorescence—Immunofluorescence was performed according to standard procedures (44). Briefly, cells were grown on coverslips. After incubation with the examined agent, cells were fixed using ice-cold methanol for 15 min and permeabilized with 0.25% Triton X-100 for 10 min at 20 °C. After blocking with a PBS solution containing 1% bovine serum albumin (BSA), fixed cells were incubated with rabbit anti-LC3 (catalog number MBPM036, Abacus-ALS), mouse anti-cathepsin D (catalog number ab72915, Abcam), or mouse anti-LAMP-2 (catalog number ab25631, Abcam) antibody in PBS (1% BSA) at 4 °C overnight. The slides were then washed in PBS and incubated with an anti-rabbit IgG (heavy + light) antibody coupled to FITC (Invitrogen) or anti-mouse IgG antibody coupled with Texas Red (Abcam) for 2 h at 20 °C. Coverslips were mounted

TABLE 1
List of primer sets, expected product size, and PCR programs
F, forward; R, reverse.

Gene	Accession number	Species	Primers (5′–3′)	Product size	Program (temperature/cycles)
				bp	
LC3	NM_022818.4	Human	F, CAGCATCCAACCAAAATCCC R, CACTGACAATTTCATCCCGAAC	300	56 °C/28
p62	NM_003900	Human	F, AGGACGGGGACTTGGTTG R, GGCGGGAGATGTGGGTAC	955	54 °C/26
β-Actin	NM_001101.3	Human	F, CCCGCCGCCAGCTCACCATGG R, AAGGTCTCAAACATGATCTGGGTC	397	56 °C/24

on glass slides using ProLong® Gold antifade reagent with DAPI (Invitrogen). Stained samples were examined with an Olympus AxioObserver Z1 fluorescence microscope (Olympus, Mt. Waverley, Victoria, Australia) by a 63× oil objective. Images were captured with AxioVision Rel 4.8 software (Carl Zeiss, Australia). Scatter plots and Mander's overlap coefficient (*r*) were generated and calculated, respectively, using NIH ImageJ.

Assessment of Lysosomal Membrane Permeability—The distribution of acridine orange (Sigma-Aldrich) was assessed to determine the integrity of the lysosomal membrane as reported previously (27). After incubation with the examined agent, cells were incubated for 15 min at 37 °C with acridine orange (20 nM) and washed three times with PBS. Fluorescence intensity was examined using the microscope described above and quantified by flow cytometry (FACSCanto, BD Biosciences) (27). Data analysis was performed using FlowJo software (Tree Star Inc., Ashland, OR).

Down-regulation of Protein Expression Using RNA Interference—Cells grown for 24 h were transfected with ON-TARGETplus siRNA oligos (Dharmacon, Lafayette, CO) for 6 h at 37 °C using Lipofectamine 2000 (Invitrogen) according to the manufacturer's instructions. Then the cells were further incubated in normal growth medium supplemented with FCS for an additional 72 h at 37 °C prior to further experiments. The following siRNAs were purchased from Dharmacon: non-targeting control siRNA (negative control siRNA, D-001810-01), human *ATG5* siRNA (J-004374-07), and human *BECN1* siRNA (J-0105552-05).

Annexin V Binding Assay—Cells were harvested with PBS-EDTA and then stained with an annexin V-FITC apoptosis detection kit (Abcam) according to the manufacturer's protocol. Stained cells were analyzed using the flow cytometer described previously.

Statistical Analysis—Data are expressed as mean ± S.D. of three experiments. Experimental data were compared using Student's *t* test. Results were considered statistically significant when p was <0.05.

RESULTS

Dp44mT and DFO Increase LC3-II Levels and Autophagosome Formation at High Doses Along with Marked Antiproliferative Activity—To investigate the levels of autophagy in response to the cytotoxic effects of the ligands Dp44mT and DFO, studies first examined the antiproliferative activity of these agents and their ability to induce autophagy markers. The human MCF7 breast cancer cell line was used initially because autophagy has been well characterized in this cell line (45). In these investigations, Dp44mT was used at low concentrations of up to 5 μM because of its high membrane permeability and marked iron chelation efficacy (20). In contrast, DFO was used at higher concentrations of up to 250 μM because of its low membrane permeability and lower iron chelation efficacy (19). Furthermore, the well established anticancer agent tamoxifen (TAM) was implemented as a positive control because of its well characterized ability to induce autophagy in estrogen receptor-positive MCF7 cells (46–48).

After a 24- and 48-h incubation, Dp44mT (5 μM) induced significantly ($p < 0.001–0.05$) greater antiproliferative activity than TAM (10 μM) or DFO (250 μM; Fig. 1, *A* and *B*). To determine whether autophagy was induced by the chelators, the conversion of LC3-I (cytosolic form) to LC3-II (autophagosome membrane-bound form) was examined (49, 50). In all studies below, LC3-II was quantified densitometrically from Western blots as it is a classical marker of autophagosome formation (49, 50). The positive control, TAM (10 μM), induced a significant ($p < 0.001$) increase in LC3-I and especially LC3-II levels relative to control cells after a 24- and 48-h incubation (Fig. 1, *C* and *D*).

After an incubation of either 24 or 48 h, the lower concentrations of Dp44mT (0.01 and 0.1 μM) either had no significant ($p > 0.05$) effect or slightly decreased LC3-I or LC3-II expression relative to the control. In contrast, Dp44mT at 5 μM markedly and significantly ($p < 0.001–0.01$) increased LC3-I and LC3-II expression *versus* the control (Fig. 1, *C* and *D*). Incubation of cells with DFO (5–250 μM) for 24 h had no significant effect on LC3-I or LC3-II levels relative to the control, whereas after 48 h, DFO at 50 or 250 μM induced a pronounced and significant ($p < 0.01–0.05$) increase in both LC3 isoforms. The increase in LC3-I and -II expression after incubation with Dp44mT and DFO (Fig. 1, *C* and *D*) occurred at high doses along with marked antiproliferative activity (Fig. 1, *A* and *B*).

Subsequently, the intracellular distribution of LC3 was visualized by fluorescence microscopy to examine the presence of autophagosome-associated LC3 (*i.e.* LC3-II) that forms a punctate pattern in the cytoplasm (49, 50). Consistent with the Western blots, TAM (10 μM) and Dp44mT (5 μM) enhanced the punctate fluorescent pattern of autophagosome-associated LC3-II relative to the control after 24 and 48 h, whereas DFO (250 μM) enhanced this only after 48 h (Fig. 1*E*). Two positive controls were utilized in these experiments, namely the late stage autophagic inhibitors bafilomycin A1 (Baf A1; 100 nM) and chloroquine (10 μM) (49, 51). Both of these agents resulted

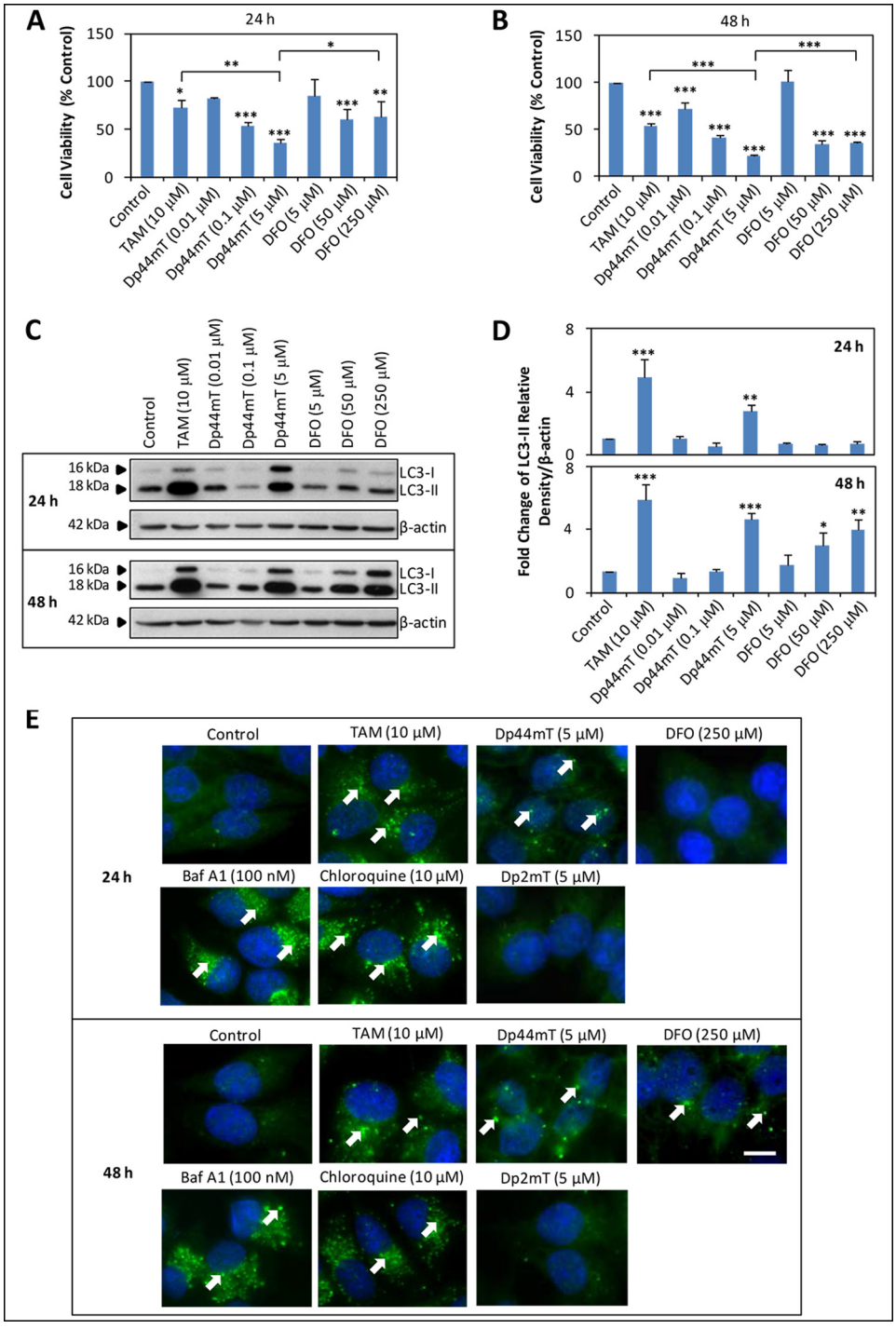

FIGURE 1. **TAM, Dp44mT, and DFO increase the expression of the classical marker of autophagy, LC3-II, in correlation with their antiproliferative activity in MCF7 cells.** *A* and *B*, cell viability of MCF7 cells incubated with either TAM (10 μM), Dp44mT (0.01, 0.1, and 5 μM), or DFO (5, 50, and 250 μM) after a 24- (*A*) or 48-h incubation (*B*). *C*, Western blotting was performed to investigate the alteration of LC3-I/II expression after a 24- or 48-h incubation of cells with the same agents in *A* and *B*. *D*, densitometric analysis (arbitrary units) of the results in *C*. *E*, immunofluorescence studies detecting LC3 in cells after a 24- or 48-h incubation with TAM (10 μM), Dp44mT (5 μM), DFO (250 μM), Baf A1 (100 nM), chloroquine (10 μM), or Dp2mT (5 μM). *Scale bar*, 10 μm. Results in *A* and *B* are the mean of three experiments with *error bars* representing S.D. Blots shown in *C* are typical of three experiments. Densitometric analysis in *D* is the mean of three experiments with *error bars* representing S.D. *, $p < 0.05$; **, $p < 0.01$; ***, $p < 0.001$ *versus* the control. Immunofluorescence photographs in *E* are representative from three experiments.

in an accumulation of LC3II-containing autophagosomes (Fig. 1*E*). The negative control compound, Dp2mT, which has a similar structure to Dp44mT but is unable to bind metals (20, 27, 44, 52), did not alter the punctate fluorescence pattern of LC3-II relative to control after 24 and 48 h (Fig. 1*E*). Collectively, Dp44mT and DFO induced an increase in LC3-II levels, reflecting an increase in autophagosome formation.

Dp44mT, but Not TAM or DFO, Induces Autophagosome Synthesis—The levels of LC3-II are known to correlate with autophagosome abundance (49, 50). However, alterations in

total LC3-II levels can result from increased synthesis and/or decreased degradation of autophagosomes (49, 50). Hence, autophagic flux was measured as it encompasses both the formation and degradation of autophagosomes (49, 50). To determine this, LC3-II levels were measured under conditions where autophagosome degradation was blocked by Baf A1 (100 nM) (49, 50).

To understand the effect of Baf A1, it is important to note that when basal levels of autophagy occur the synthesis of LC3-II is in equilibrium with its autophagic degradation. When the autophagosome is degraded after it binds to the lysosome, LC3-II levels remain unchanged (Fig. 2*A*, *i*). However, in the presence of Baf A1, autophagosome degradation and autophagosome-lysosome fusion are inhibited (49, 53), leading to accumulation of LC3-II (Fig. 2*A*, *ii*). When an autophagy inducer is introduced, autophagosome synthesis is increased relative to the basal state, resulting in increased LC3-II accumulation when degradation is blocked by Baf A1 (Fig. 2*A*, *iii*). If the increase in LC3-II by an agent was only due to inhibition of autophagosome turnover, the addition of Baf A1 in the presence of this agent would not be expected to lead to a further increase in LC3-II when compared with the basal state in the presence of Baf A1. Thus, by blocking the degradation stage of autophagy with Baf A1, the extent of autophagosome formation in response to a particular agent can be determined (49, 50) (Fig. 2*A*).

To assess autophagosome formation, MCF7 cells were incubated for 24 or 48 h with either control medium, TAM (10 μM), Dp44mT (5 μM), or DFO (250 μM) in the absence or presence of Baf A1. Under control conditions, Baf A1 induced a significant ($p < 0.001$) increase in LC3-II levels relative to control cells incubated in the absence of this inhibitor, and this represents basal autophagosome formation (49, 50) (Fig. 2, *B* and *C*). A significant ($p < 0.001$) increase in LC3-II levels by TAM was observed compared with control cells in the absence of Baf A1 after a 24- and 48-h incubation (Fig. 2, *B* and *C*). However, there was no significant ($p > 0.05$) change in LC3-II levels when TAM was co-incubated with Baf A1 compared with control cells incubated with Baf A1 alone (Fig. 2, *B* and *C*). This observation suggests that TAM does not affect autophagosome formation. Hence, in the absence of Baf A1, the increased expression of LC3-II after incubation with TAM is probably due to decreased degradation of autophagosomes (this is examined further in the next section by assessing p62 levels).

Incubation with Dp44mT led to a significant ($p < 0.001$–0.05) increase in LC3-II levels compared with control cells in the absence of Baf A1 after both a 24- and 48-h incubation (Fig. 2, *B* and *C*). Dp44mT also significantly ($p < 0.01$) increased LC3-II levels in the presence of Baf A1 relative to control cells incubated with Baf A1 alone after both 24 and 48 h (Fig. 2, *B* and *C*). This finding is in contrast to that found for TAM and suggests that the rate of autophagosome formation is increased by Dp44mT, which was also observed at the earlier time point of 8 h (Fig. 2, *D*–*G*). The observation that Dp44mT increases autophagic flux was further examined by utilizing another well characterized late stage autophagic inhibitor, namely chloroquine (49, 51). This latter inhibitor was found to produce an effect similar to Baf A1, but its inhibition of autophagy was not as marked as Baf A1 (data not shown) as found in previous studies from our laboratory (54).

In contrast to TAM and Dp44mT, no significant ($p > 0.05$) change in LC3-II level was observed after incubation with DFO relative to the control in the absence of Baf A1 after 8 or 24 h (Fig. 2, *B*–*E*). Conversely, a significant ($p < 0.05$) increase in LC3-II was found after a 48-h incubation with DFO *versus* the control (Fig. 2, *B* and *C*). However, there was no significant ($p > 0.05$) change in LC3-II levels when DFO was co-incubated with Baf A1 compared with control cells incubated with Baf A1 alone after both a 24- and 48-h incubation (Fig. 2, *B* and *C*). Similar to TAM, it can be rationalized that DFO inhibits autophagosome degradation, which leads to LC3-II accumulation. This observation is speculatively due to these agents inhibiting the fusion of autophagosomes to lysosomes or rendering the lysosomes inactive.

The results above demonstrate that Dp44mT relative to TAM and DFO induce initiation of autophagosome synthesis as determined by LC3-II levels in the presence of Baf A1 (Fig. 2, *B* and *C*). Considering this observation, studies then examined *LC3* mRNA levels after incubation with these agents. In agreement with LC3-II expression in the presence of Baf A1 (Fig. 2, *B* and *C*), Dp44mT induced a significant ($p < 0.001$) increase in *LC3* mRNA after a 24- or 48-h incubation *versus* the control (Fig. 3, *A* and *B*). In contrast, no significant ($p > 0.05$) alteration in *LC3* mRNA was observed with TAM or DFO relative to the control (Fig. 3, *A* and *B*). These results at the mRNA level confirm the findings at the protein level that Dp44mT induced autophagosome synthesis, whereas TAM or DFO inhibited autophagosome degradation (Fig. 2, *B* and *C*).

Dp44mT Increases p62 Due to Decreased Autophagosome Degradation—Another classical autophagy substrate and receptor, namely p62 (55), has been used previously by other investigators to monitor autophagic flux (*i.e.* the rate at which the autophagic process is completed) (56, 57). Of note, p62 is selectively incorporated into autophagosomes through direct binding to LC3-II and is degraded by autophagy (Fig. 4*A*, *i*) (55). An induction of the autophagic flux leads to increased degradation of p62 (Fig. 4*A*, *ii*), whereas an impaired autophagic flux (*i.e.* inhibition of autophagosome degradation) will result in an accumulation of p62 (Fig. 4*A*, *iii*) (55). In Fig. 4*B*, Western blots showing LC3-II expression have been added to complement the p62 expression for easier interpretation. These LC3-II results are similar to those shown in Fig. 1, *C* and *D*.

After a 24- or 48-h incubation, TAM (10 μM) induced a significant ($p < 0.001$–0.05) increase in p62 level relative to the control (Fig. 4, *B* and *C*). This observation supports the results in Fig. 2, *B* and *C*, demonstrating that despite increased LC3-II levels by TAM no change in LC3-II level occurred after incubation with TAM plus the autophagosomal degradation inhibitor Baf A1 relative to the control and Baf A1. Hence, together the results examining autophagic flux via the use of Baf A1 (Fig. 2, *B* and *C*) and p62 accumulation (Fig. 4, *B* and *C*) indicate that the TAM-induced increase in LC3-II levels was due to inhibition of autophagosomal degradation.

Only the highest concentrations of Dp44mT (0.1 and 5 μM) induced a significant ($p < 0.001$–0.01) increase in p62 levels after 24 and 48 h (Fig. 4, *B* and *C*). These findings suggest

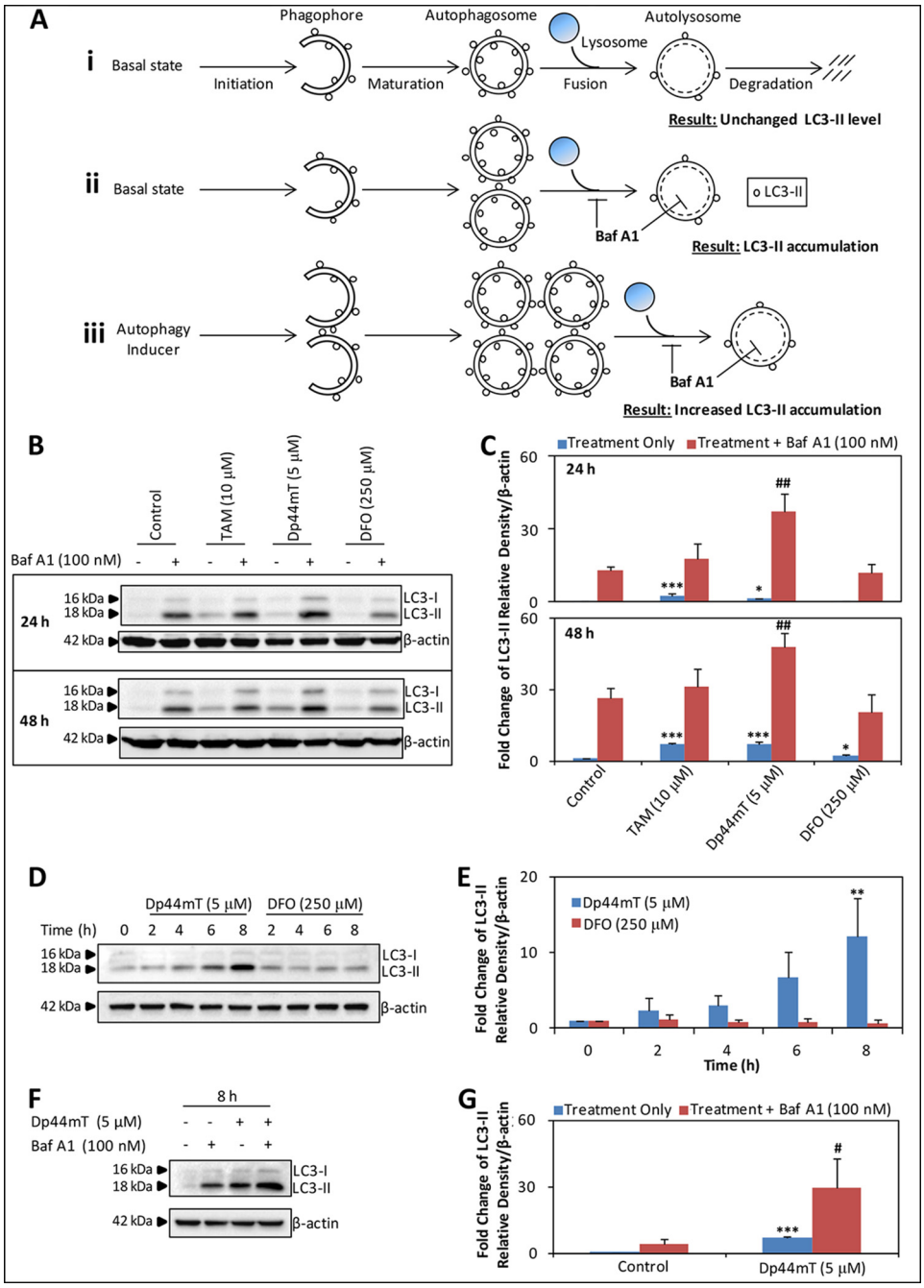

FIGURE 2. **Dp44mT, but not DFO, induces autophagic initiation.** *A*, schematics depicting alterations in total LC3-II levels that can result from increased synthesis and/or decreased degradation of autophagosomes. *i*, when autophagy occurs in the basal state, the autophagosome formed is degraded after it fuses with the lysosome, leaving LC3-II levels unchanged. *ii*, in the presence of Baf A1 (100 nM), autophagosome degradation and autophagosome-lysosome fusion are inhibited. This leads to LC3-II accumulation, which reflects the extent of autophagosome formation in response to a particular agent. *iii*, when autophagosome degradation is blocked by Baf A1 and an autophagy inducer is introduced, autophagosome synthesis is increased relative to the basal state, resulting in increased LC3-II accumulation. *B*, MCF7 cells were preincubated with control medium or medium containing Baf A1 (100 nM) for 30 min at 37 °C followed by a 24- or 48-h 37 °C incubation with either control medium or medium with Baf A1 (100 nM) in the presence or absence of either TAM (10 μM), Dp44mT (5 μM), or DFO (250 μM). Western blotting was performed to investigate LC3-I/II expression. *C*, densitometric analysis (arbitrary units) of the results in *B*. *D*, MCF7 cells were incubated with control medium or medium containing Dp44mT (5 μM) or DFO (250 μM) for 0–8 h at 37 °C. Western blotting was performed to investigate LC3-I/II expression. *E*, densitometric analysis (arbitrary units) of the results in *D*. *F*, MCF7 cells were preincubated with control medium or medium containing Baf A1 (100 nM) for 30 min at 37 °C followed by an 8-h 37 °C incubation with Dp44mT (5 μM) alone, Baf A1 (100 nM) alone, or both in combination. Western blotting was performed to investigate LC3-I/II expression. *G*, densitometric analysis (arbitrary units) of the results in *F*. Blots shown are representative of three experiments. Densitometric analysis is the mean of three experiments with *error bars* representing S.D. *, $p < 0.05$; **, $p < 0.01$; ***, $p < 0.001$ *versus* the control. #, $p < 0.05$; ##, $p < 0.01$ *versus* Baf A1 alone.

decreased degradation of autophagosomes after incubation with Dp44mT under these conditions. In contrast to TAM or Dp44mT, DFO did not cause any alteration in p62 expression relative to the control after a 24-h incubation (Fig. 4, *B* and *C*). However, after 48 h, the highest concentrations of DFO (50 and 250 μM) induced a significant ($p < 0.01$–0.05) increase in p62 level compared with the control (Fig. 4, *B* and *C*). Similar to TAM, DFO did not cause an increase in LC3-II level in the

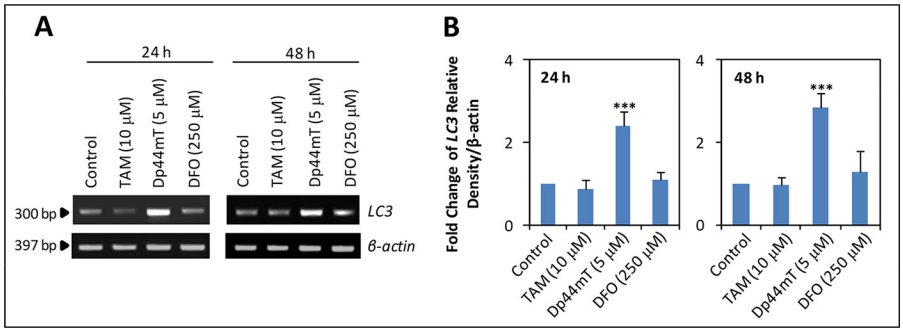

FIGURE 3. **Dp44mT increases *LC3* mRNA level after a 24- or 48-h incubation.** *A*, MCF7 cells were incubated with either TAM (10 μM), Dp44mT (5 μM), or DFO (250 μM) for 24 or 48 h at 37 °C. Semiquantitative RT-PCR was performed to investigate *LC3* mRNA levels. *B*, densitometric analysis (arbitrary units) of the results in *A*. Gels shown are representative of three experiments. Densitometric analysis is the mean of three experiments with *error bars* representing S.D. ***, $p <$ 0.001 *versus* the control.

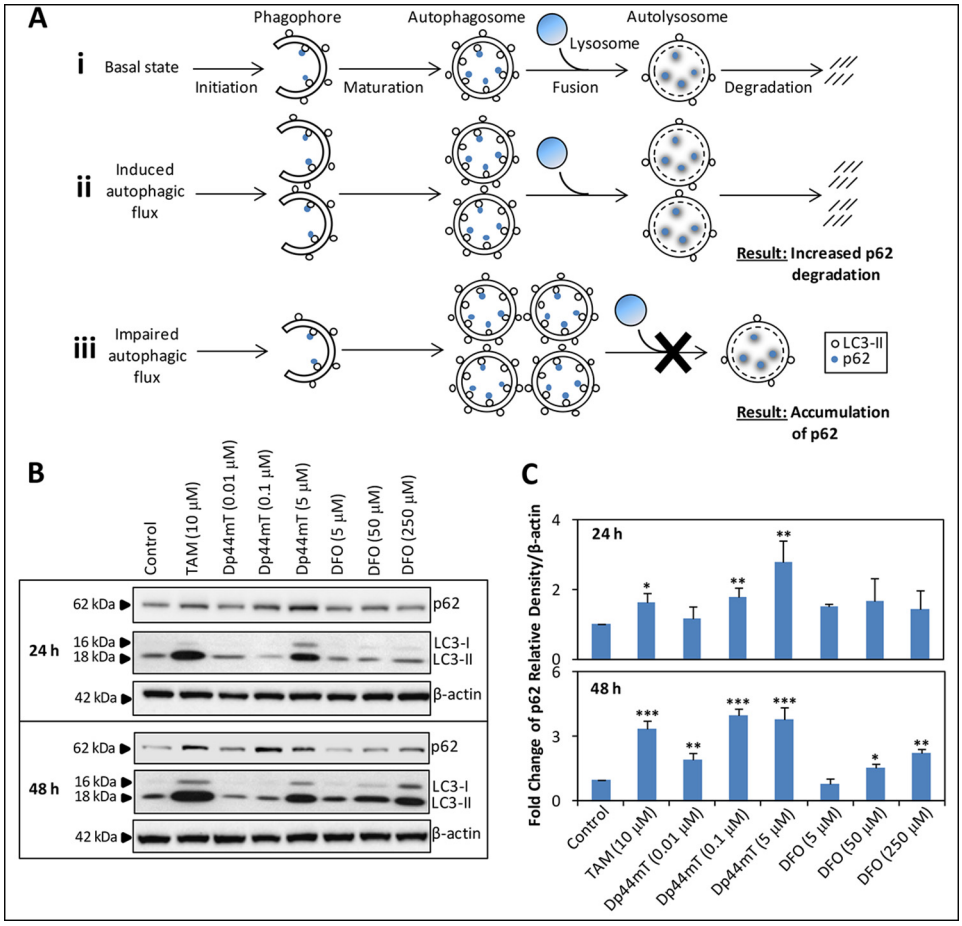

FIGURE 4. **Dp44mT and DFO suppress autophagosome degradation.** *A*, schematics showing how p62 is used to monitor autophagic flux. *i*, p62 is selectively incorporated into autophagosomes through direct binding to LC3-II and is degraded by autophagy. *ii*, when autophagic flux is induced, more autophagosomes are formed, leading to increased degradation of p62. *iii*, when autophagic flux is impaired due to inhibition of autophagosome degradation, an accumulation of p62 is observed. *B*, MCF7 cells were incubated with either TAM (10 μM), Dp44mT (0.01, 0.1, and 5 μM), or DFO (5, 50, and 250 μM) for 24 or 48 h at 37 °C. Western blotting was performed to investigate the alteration of p62 and LC3-II expression. *C*, densitometric analysis (arbitrary units) of p62 Western blots in *B*. Blots shown are representative of three experiments. Densitometric analysis is the mean of three experiments with *error bars* representing S.D. *, $p <$ 0.05; **, $p < 0.01$; ***, $p < 0.001$ *versus* the control.

presence of Baf A1 compared with cells incubated with Baf A1 alone after 24 or 48 h (Fig. 2, *B* and *C*). Therefore, the increase in LC3-II expression after incubation with DFO was due to a reduction in autophagosome degradation.

Dp44mT Increases p62 mRNA Due to Increased Transcription—An increase in p62 protein level (Fig. 4, *B* and *C*) may result in part from the up-regulation of *p62* mRNA levels. Studies examining *p62* mRNA expression demonstrated that only Dp44mT significantly ($p < 0.001$) increased its levels after 24 or 48 h (Fig. 5, *A* and *B*). To determine whether the Dp44mT-induced increase in *p62* mRNA was due to increased transcription rather than increased mRNA half-life, the cells were pre-incubated for 2 h in the presence or absence of the transcription inhibitor actinomycin D (Act D; 4 μM) (43). This procedure was

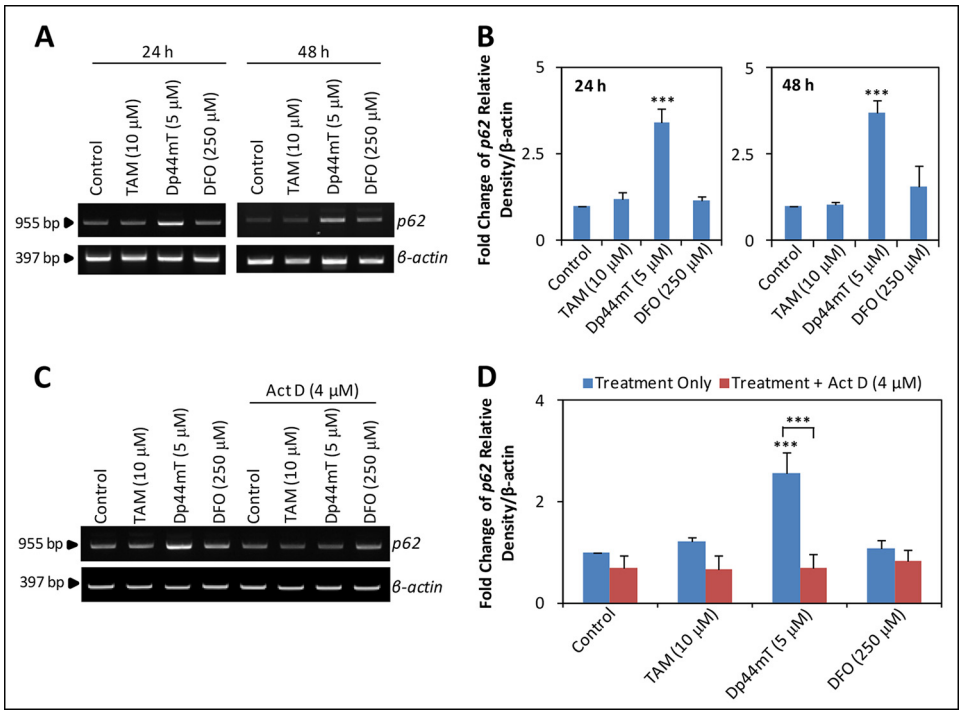

FIGURE 5. **Dp44mT up-regulates *p62* mRNA levels.** *A*, MCF7 cells were incubated with either TAM (10 μM), Dp44mT (5 μM), or DFO (250 μM) for 24 or 48 h at 37 °C. Semiquantitative RT-PCR was performed to investigate *p62* mRNA levels. *B*, densitometric analysis (arbitrary units) of the results in *A*. *C*, MCF7 cells were preincubated with either control medium or medium containing Act D (4 μM) for 2 h at 37 °C followed by a 6-h 37 °C incubation with either control medium or medium containing TAM (10 μM), Dp44mT (5 μM), or DFO (250 μM) in the presence or absence of Act D (4 μM). Semiquantitative RT-PCR was performed to investigate *p62* mRNA levels. *D*, densitometric analysis (arbitrary units) of the results in *C*. Gels shown are representative of three experiments. Densitometric analysis is the mean of three experiments with *error bars* representing S.D. ***, $p < 0.001$ *versus* the control.

then followed by reincubation with the agents for 6 h in the presence or absence of Act D (4 μM). A shorter incubation time point was implemented as the high doses of Act D used to markedly inhibit transcription are cytotoxic over longer periods (58). Only Dp44mT significantly ($p < 0.001$) up-regulated *p62* mRNA, and this was inhibited by Act D (Fig. 5, *C* and *D*). These results suggested that the initial Dp44mT-mediated increase in *p62* mRNA was due to increased transcription. Because of the limitations of using Act D after long incubations, we cannot exclude that at later time points (*i.e.* 24 or 48 h) there are changes in *p62* mRNA stability.

Dp44mT Increases Autophagosome Synthesis and Decreases Autophagosomal Degradation in Multiple Cell Types—As shown previously using Baf A1, Dp44mT caused an increase in LC3-II-containing autophagosome synthesis relative to the Baf A1-treated control (Fig. 2, *B* and *C*). Hence, the intracellular accumulation of p62 after incubation with Dp44mT (Fig. 4, *B* and *C*) indicates that the increased autophagic flux is not sufficient to fully clear this substrate and could be due to a simultaneous decrease in autophagosome degradation. This increased rate of autophagosome formation in the presence of Dp44mT (as rationalized from the increased LC3-II in the presence of Baf A1 relative to the control plus Baf A1) and p62 accumulation were also observed after the breast cancer cell lines MDA-MB-231 and T47D were incubated with Dp44mT (Fig. 6, *A–F*). These observations indicate that this effect of Dp44mT was not just specific for MCF7 cells.

The Redox-active Iron or Copper Complexes of Dp44mT Increase Autophagosome Synthesis and Decrease Autophagosome Degradation—Next we examined the mechanism of action by which Dp44mT increases autophagosome synthesis and decreases autophagosome degradation. Initially, the well characterized ability of the chelators to bind cellular iron (19, 20) was assessed in terms of their efficacy in increasing LC3-II expression. The negative control compound, Dp2mT (20, 27, 44, 52), did not significantly alter LC3-I or LC3-II levels compared with the control (Fig. 7, *A* and *B*). Similarly, Dp2mT (5 μM) did not induce any significant ($p > 0.05$) change in p62 level relative to the control (Fig. 7, *A* and *B*). Considering these data with Dp2mT relative to those with Dp44mT, it can be concluded that metal ion binding plays an important role in the increased autophagosome formation and inhibition of autophagosome degradation by Dp44mT.

Incubation with the Dp44mT·iron complex ($Fe[Dp44mT]_2$) induced LC3-II to a level that was significantly ($p < 0.01–0.05$) greater than the control after 24 or 48 h (Fig. 7, *A* and *B*). Hence, this result suggested that the iron complex itself and/or its redox activity (39) induced autophagy. However, the effect of $Fe[Dp44mT]_2$ at increasing LC3-II expression was significantly ($p < 0.001–0.05$) less than that found when cells were incubated with Dp44mT alone after 24 or 48 h (Fig. 7, *A* and *B*). Similar observations were also found for p62 with both Dp44mT and $Fe[Dp44mT]_2$ significantly ($p < 0.05–0.01$) inducing expression after 24 or 48 h (Fig. 7, *A* and *B*). No significant ($p > 0.05$) alteration was observed with $Fe[Dp44mT]_2$ relative to Dp44mT alone (Fig. 7, *A* and *B*). In contrast to $Fe[Dp44mT]_2$, the DFO·iron complex (Fe[DFO]) did not significantly ($p > 0.05$) increase the levels of LC3-II after 24 or 48h relative to control. Moreover, the LC3-II level after a 48-h incu-

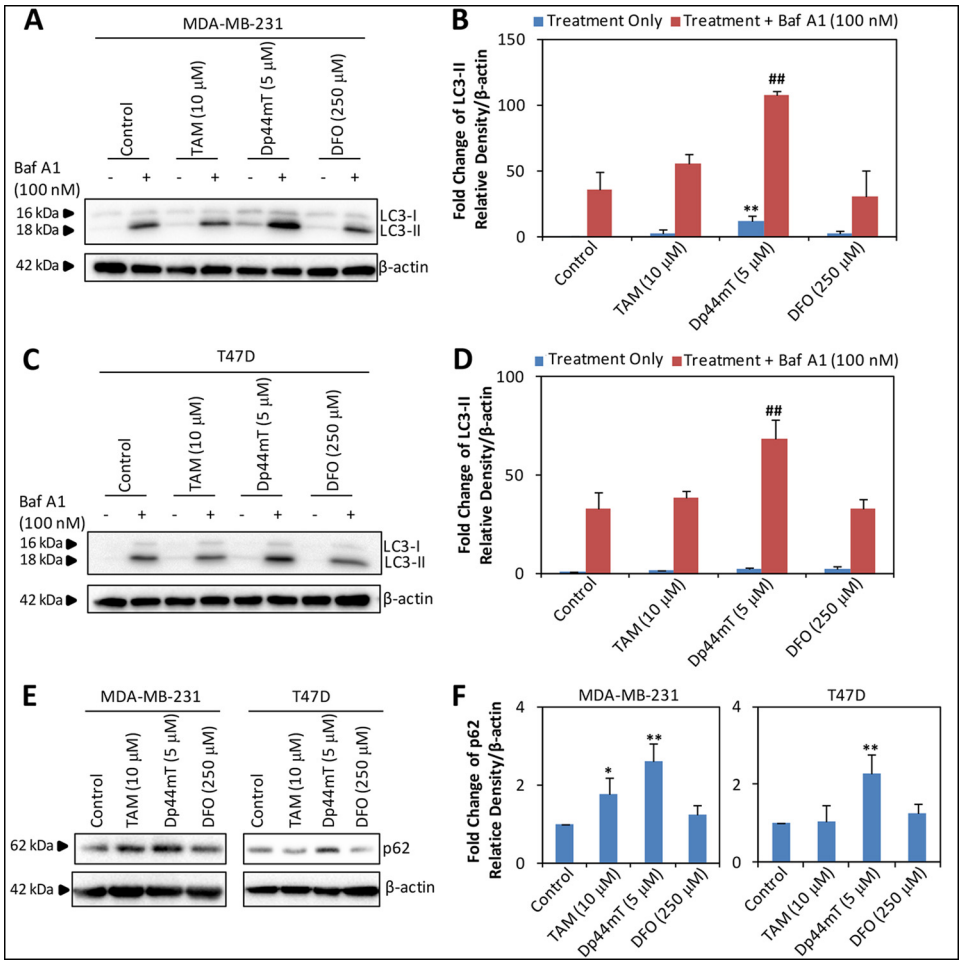

FIGURE 6. **Dp44mT induces autophagic initiation and suppresses autophagosome degradation in MDA-MB-231 and T47D breast cancer cell lines.** *A*, MDA-MB-231 cells were preincubated with control medium or medium containing Baf A1 (100 nM) for 30 min at 37 °C followed by a 24-h 37 °C incubation with control medium or medium containing TAM (10 μM), Dp44mT (5 μM), or DFO (250 μM) in the presence or absence of Baf A1 (100 nM). Western blotting was performed to investigate LC3-I/II expression. *B*, densitometric analysis (arbitrary units) of the results in *A*. *C*, T47D cells were preincubated and incubated in the same conditions as in *A*. Western blotting was performed to investigate LC3-I/II expression. *D*, densitometric analysis (arbitrary units) of the results in *C*. *E*, MDA-MB-231 or T47D cells were incubated with either TAM (10 μM), Dp44mT (5 μM), or DFO (250 μM) for 24 h at 37 °C. Western blotting was performed to investigate the alteration of p62 expression. *F*, densitometric analysis (arbitrary units) of results in *E*. Blots shown are representative of three experiments. Densitometric analysis is the mean of three experiments with *error bars* representing S.D. *, $p < 0.05$; **, $p < 0.01$ *versus* the control. ##, $p < 0.01$ *versus* Baf A1 alone.

bation with Fe[DFO] was significantly ($p < 0.01$) less than that found when cells were incubated with DFO alone (Fig. 7, *A* and *B*). DFO and Fe[DFO] induced a slight but significant ($p < 0.05$) increase in p62 level after a 48-h incubation relative to the control (Fig. 7, *A* and *B*). However, no significant ($p > 0.05$) alteration was observed comparing Fe[DFO] relative to DFO alone (Fig. 7, *A* and *B*). The relative control for the iron complexes, namely $FeCl_3$, did not result in any significant ($p > 0.05$) alteration in LC3-II or p62 expression relative to the control (Fig. 7, *A* and *B*). Collectively, these observations suggest that the ability of Dp44mT and DFO to bind cellular iron is important for increasing LC3-II expression.

It could be suggested that the ability of Dp44mT to increase LC3-II or p62 levels was not solely due to binding iron but also other metal cations in the cell. Previous studies have shown that Dp44mT also binds copper, which plays an important role in its antiproliferative activity (27, 28). When Dp44mT was complexed with copper (Cu[Dp44mT]; 5 μM), a marked and significant ($p < 0.001$) increase in LC3-II level was observed relative to that induced by Dp44mT alone (Fig. 7, *C* and *D*). In contrast, at lower concentrations (*i.e.* 0.1 μM), Dp44mT or Cu[Dp44mT] had no significant effect on LC3-II expression *versus* the control (Fig. 7, *C* and *D*). Similar observations were also found when p62 levels were assessed except that Dp44mT and Cu[Dp44mT] significantly ($p < 0.001–0.05$) increased its levels relative to the control at both 0.1 and 5 μM (Fig. 7, *C* and *D*). These observations indicated that the formation of Cu[Dp44mT] could also be important for the increase in LC3-II and p62 expression found after cells were incubated with Dp44mT. As a control for the effects of free copper in experiments involving the Cu[Dp44mT] complex, cells were incubated with $CuCl_2$ (5 μM), which had no significant ($p < 0.05$) effect on LC3-II or p62 levels (Fig. 7, *C* and *D*).

Unlike DFO, which forms a redox-inactive iron complex (9), Dp44mT forms cytotoxic, redox-active iron and copper complexes that induce ROS generation (20, 39) and lead to the depletion of the major cellular antioxidant, glutathione (27). Therefore, it was crucial to determine whether the redox-active

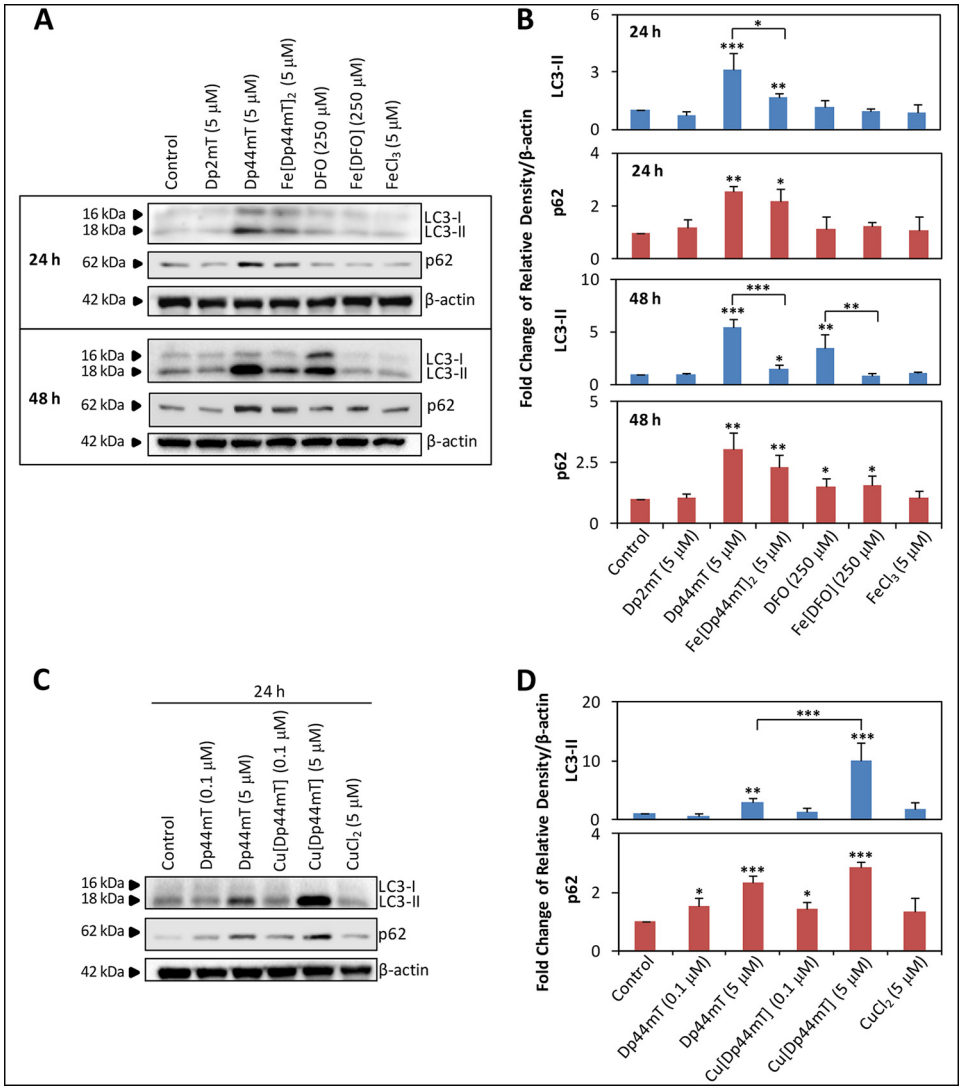

FIGURE 7. **Dp44mT binds iron or copper to induce elevated LC3-II levels.** *A*, MCF7 cells were incubated with control medium or medium containing Dp2mT (5 μM), Dp44mT (5 μM), $Fe[Dp44mT]_2$ (5 μM), DFO (250 μM), Fe[DFO] (250 μM), or $FeCl_3$ (5 μM) alone for 24 or 48 h at 37 °C. Western blotting investigated LC3-I/II and p62 expression. *B*, densitometric analysis (arbitrary units) of the results in *A*. *C*, MCF7 cells were incubated for 24 h at 37 °C with control medium or medium containing Dp44mT (0.1 and 5 μM), Cu[Dp44mT] (0.1 and 5 μM), or $CuCl_2$ (5 μM) for 24 h at 37 °C. Western blotting was performed to investigate LC3-I/II and p62 expression. *D*, densitometric analysis (arbitrary units) of the results in *C*. Blots shown are representative of three experiments. Densitometric analysis is the mean of three experiments with *error bars* representing S.D. *, $p < 0.05$; **, $p < 0.01$; ***, $p < 0.001$ *versus* the control or between treatments as indicated.

nature of Dp44mT was important in terms of its ability to induce autophagy. To examine this, cells were incubated with Dp44mT in the presence or absence of *N*-acetylcysteine (NAC; 10 mM). NAC has been shown to be a precursor to H_2S and persulfides (59, 60) as well as a precursor of glutathione for maintaining the redox state of the cell (61, 62). Moreover, NAC was reported to reduce the cytotoxicity of Dp44mT (27). When assessing autophagic flux using Baf A1, the increase in LC3-II level induced by Dp44mT in the presence of Baf A1 was significantly ($p < 0.001$) reduced when Dp44mT was co-incubated with NAC (Fig. 8, *A* and *B*). Conversely, NAC by itself had no significant ($p > 0.05$) effect on the basal level of LC3-II relative to the control. Collectively, these observations indicated that co-incubation of Dp44mT with NAC inhibited the increase in autophagosome synthesis induced by Dp44mT.

Additionally, p62 levels were significantly ($p < 0.01$) decreased after incubation with Dp44mT in combination with NAC relative to Dp44mT alone (Fig. 8, *C* and *D*). Again, NAC alone had no significant effect on p62 levels relative to the control (Fig. 5, *G* and *H*). Therefore, considering the results from Fig. 8, *A–D* collectively, the redox activity of Dp44mT induced autophagosome synthesis on the basis of LC3-II levels in the presence of Baf A1 but also retarded autophagosome degradation as judged by p62 expression, and both could be prevented by the cytoprotective antioxidant NAC.

Dp44mT Decreases Autophagosome Degradation by Causing Lysosomal Destabilization—As shown in earlier studies (Fig. 2, *B* and *C*), the increase in LC3-II level induced by TAM, Dp44mT, and DFO was at least in part due to inhibition of autophagosomal degradation with Dp44mT additionally increasing the rate of autophagosome formation. The lysosome plays an integral part in the degradation stage of autophagy by fusing with the autophagosome to generate the autolysosome (Fig. 2*A*, *i*) (2). Hence, these acidic vesicles were examined after

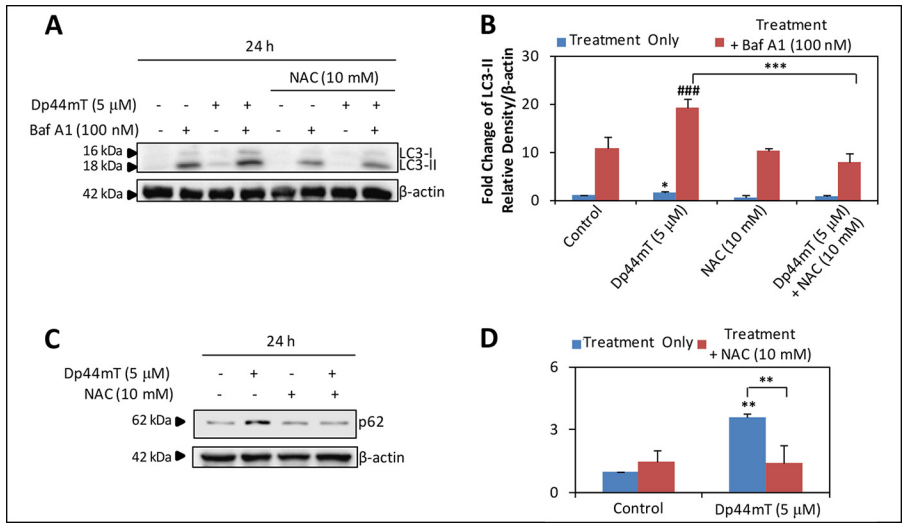

FIGURE 8. **The redox activity of Dp44mT induces autophagic initiation and decreases autophagosome degradation.** *A*, MCF7 cells were preincubated with either control medium or medium containing NAC (10 mM) alone, Baf A1 (100 nM) alone, or NAC (10 mM) + Baf A1 (100 nM) for 30 min at 37 °C followed by a 24-h 37 °C incubation with either control medium or medium containing Dp44mT (5 μM), Baf A1 (100 nM), Dp44mT (5 μM) + Baf A1 (100 nM), NAC (10 mM) alone, NAC (10 mM) + Baf A1 (100 nM), Dp44mT (5 μM) + NAC (10 mM), or Dp44mT (5 μM) + NAC (10 mM) + Baf A1 (100 nM). Western blotting was performed to investigate LC3-I/II expression. *B*, densitometric analysis (arbitrary units) of the results in *A*. *C*, MCF7 cells were preincubated with control medium or medium containing NAC (10 mM) for 30 min at 37 °C followed by a 24-h 37 °C incubation with control medium or medium containing Dp44mT (5 μM) alone, NAC (10 mM) alone, or Dp44mT (5 μM) + NAC (10 mM). Western blotting was performed to investigate p62 expression. *D*, densitometric analysis (arbitrary units) of the results in *C*. Blots shown are representative of three experiments. Densitometric analysis is the mean of three experiments with *error bars* representing S.D. *, $p < 0.05$; **, $p < 0.01$; ***, $p < 0.001$ *versus* the control or between treatments as indicated. ###, $p < 0.001$ *versus* Baf A1 alone.

incubation with these agents. This was initially assessed through the use of the lysosomotropic, metachromatic agent acridine orange (63). When acridine orange accumulates within lysosomes and autolysosomes (50) at high concentrations, it results in a red fluorescence, whereas lower cytosolic and nuclear concentrations give a green fluorescence (63). In these studies, the mean green:red fluorescence ratio was measured to determine the fractional volume of the cellular acidic compartment (64).

Examining control cells, a granular red fluorescence pattern consistent with the localization of acridine orange in lysosomes was observed together with green staining of the cytosol and nuclei (Fig. 9*A*, *panel i*) as shown previously (27, 63, 65). In contrast, incubation with TAM led to an increase in granular red fluorescence compared with the control, whereas the green staining of the cytosol remained relatively constant (Fig. 9*A*, *panel i*). This was reflected by the slight, but not significant, decrease of the mean green:red fluorescence ratio after incubation with TAM compared with the control (Fig. 9*A*, *panel ii*). Bright field photographs also revealed an increase in cytosolic granularity in TAM-treated cells relative to the control (Fig. 9*A*, *panel i*). These observations suggest a possible increase in the number of lysosomes/autolysosomes or an increase in the permeation/accumulation of acridine orange into these organelles after incubation with TAM (Fig. 9*A*).

Conversely, after incubation with Dp44mT, there was a marked loss of red fluorescence and an increase in green fluorescence of the nuclei and cytoplasm (Fig. 9*A*, *panel i*), resulting in a significant ($p < 0.001$) increase in the mean green:red fluorescence ratio relative to the control (Fig. 9*A*, *panel ii*). This observation was consistent with lysosomal membrane permeabilization (LMP; Fig. 9*A*) with increased release of acridine orange from lysosomes into the cytosol and nuclei (65) as shown previously (27). Bright field photographs of the same cells after incubation with Dp44mT demonstrated a marked decrease in granularity in the cytosol relative to the control cells (Fig. 9*A*, *panel i*).

Interestingly, a distinct pattern of acridine orange staining was observed after incubation with DFO (Fig. 9*A*, *panel i*). In this case, DFO slightly decreased the granular red fluorescence, but there was no marked alteration in cytosolic/nuclear green fluorescence (Fig. 9*A*, *panel i*), resulting in no significant alteration in the mean green:red fluorescence ratio compared with the control (Fig. 9*A*, *panel ii*). This finding with DFO is not consistent with LMP as a significant increase in green cytosolic/nuclear fluorescence was not observed. Bright field photography of DFO-treated cells revealed an increase in vacuolization and loss of fine granularity in the cytosol that was different from the effect mediated by Dp44mT or TAM (Fig. 9*A*, *panel i*).

The alterations in acridine orange staining induced by Dp44mT and DFO were then examined using the cytoprotective antioxidant NAC, which prevented the Dp44mT-mediated increase in p62 (Fig. 8, *C* and *D*) and lysosomal damage (27). As shown in Fig. 6*B*, NAC significantly ($p < 0.001–0.01$) reduced the ability of Dp44mT at 0.1 and 5 μM to increase the mean green:red fluorescence ratio. This finding in the presence of NAC is consistent with decreased damage to lysosomes by redox-active Dp44mT (27). In contrast to Dp44mT, NAC did not significantly affect acridine orange distribution after incubation with DFO (Fig. 9*B*). Again, this indicated that the mechanism involved in the decreased granular red staining with DFO was not consistent with redox-induced LMP (Fig. 9*B*). Certainly, it is well known that unlike the Dp44mT·metal complex, which generates ROS (20, 27, 39), the DFO·metal complex is not redox-active (9, 66) and should not damage the lysosome by this mechanism.

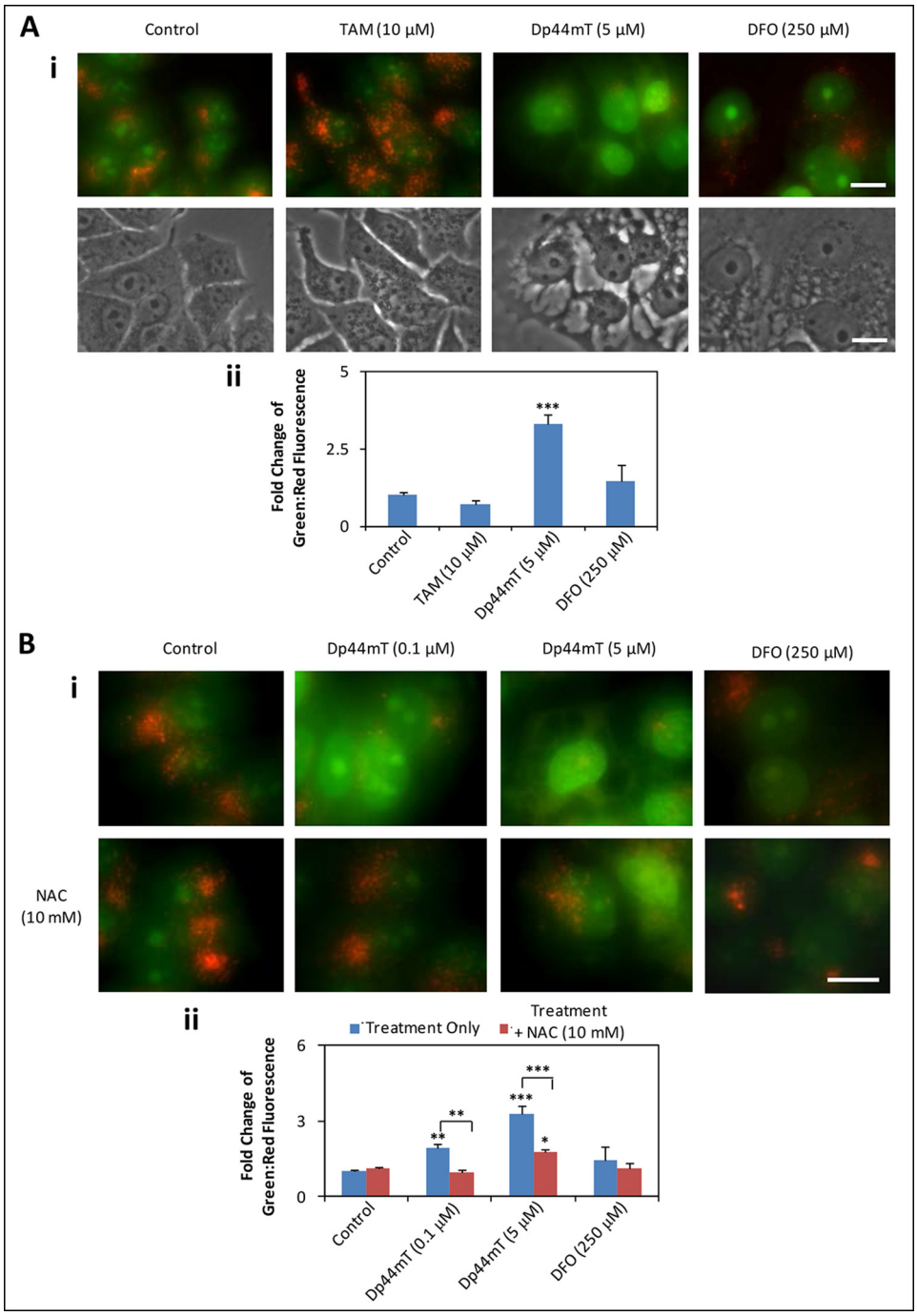

FIGURE 9. **Dp44mT decreases autophagosome degradation by causing lysosomal destabilization.** *A*, MCF7 cells were incubated with control medium or medium containing TAM (10 μM), Dp44mT (5 μM), or DFO (250 μM) for 24 h at 37 °C. *Panel i*, lysosomal integrity was shown by staining with acridine orange (20 nM) using fluorescence microscopy. Bright field photographs are shown to illustrate cell morphology under the same conditions. *Scale bars*, 10 μm. *Panel ii*, red and green fluorescence was quantified via flow cytometry. *B*, MCF7 cells were preincubated with control medium or medium containing NAC (10 mM) for 30 min at 37 °C followed by a 24-h 37 °C incubation with control medium or medium containing Dp44mT (0.1 μM), Dp44mT (5 μM), DFO (250 μM) alone, or NAC (10 mM) alone or in combination with these agents. *Panel i*, lysosomal integrity was shown by staining with acridine orange (20 nM) using fluorescence microscopy. *Scale bar*, 10 μm. *Panel ii*, red and green fluorescence was quantified via flow cytometry. Images shown are typical of three experiments. -Fold increase of the green:red fluorescence ratio is the mean of three experiments with *error bars* representing S.D. *, $p < 0.05$; **, $p < 0.01$; ***, $p < 0.001$ *versus* the control or between treatments as indicated.

The state of the lysosomes after treatment with TAM, Dp44mT, and DFO was also further examined by observing the co-localization of the lysosomal protease cathepsin D (Cat D) with lysosome-associated membrane protein 2 (LAMP-2) via immunofluorescence (Fig. 10*A*). The co-localization of Cat D and LAMP-2 in these images was analyzed using scatter plots and Mander's overlap coefficient (*r*) (67). Mander's overlap coefficient provides statistical information regarding the positional relation between biological objects and their relative intensities (68). In control cells, the punctate distribution of Cat D (*green* stain) and LAMP-2 (*red* stain) and their co-localization ($r = 0.825$) upon the merge, resulting in *yellow* stained lyso-

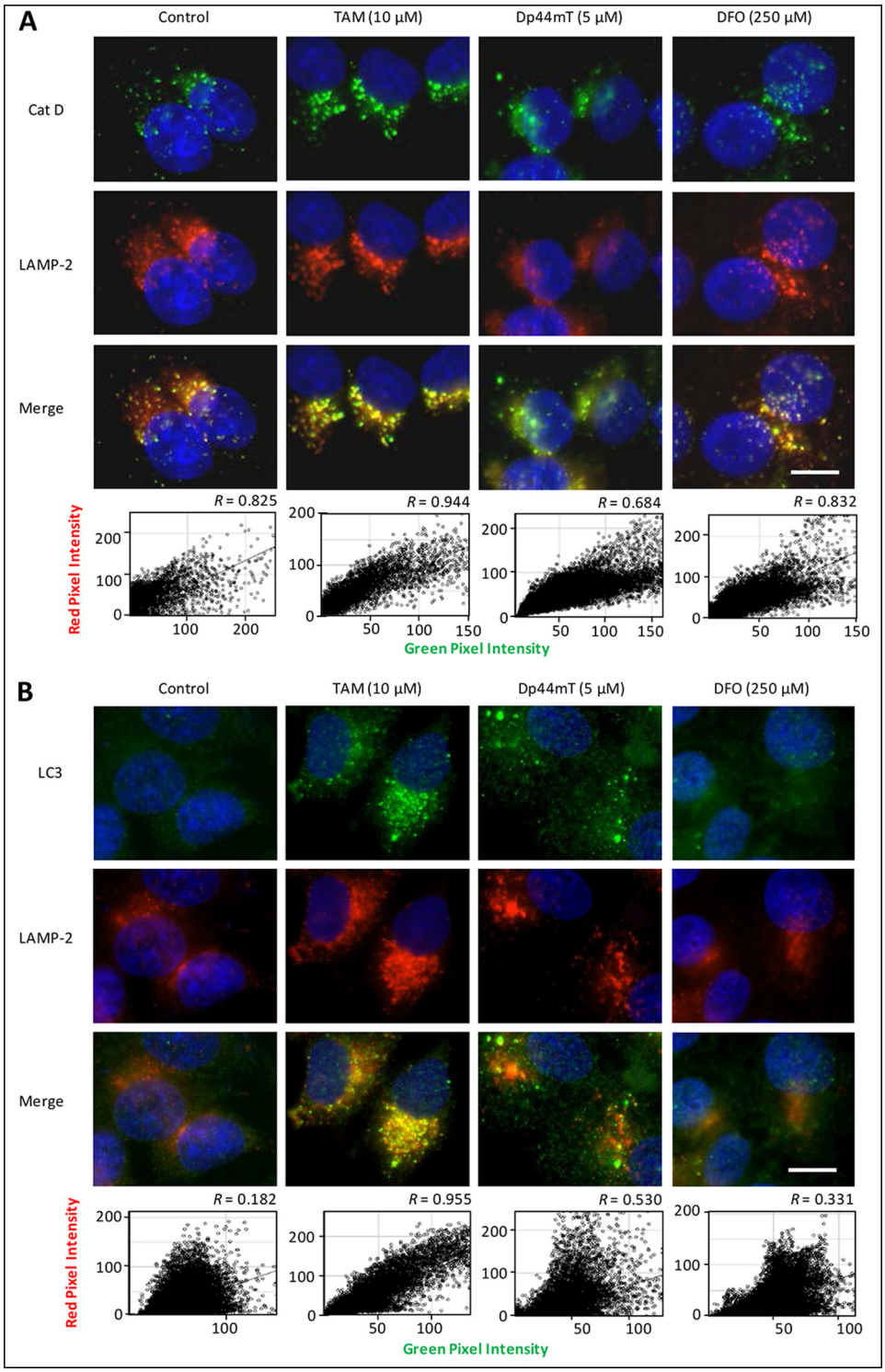

FIGURE 10. **Dp44mT disrupts co-localization of Cat D and LAMP-2, indicating lysosomal damage, and decreases co-localization of autophagosome marker LC3-II and LAMP-2.** MCF7 cells were incubated with control medium or medium containing TAM (10 μM), Dp44mT (5 μM), or DFO (250 μM) for 24 h at 37 °C. *A* and *B*, immunofluorescence studies examining the co-localization of Cat D with LAMP-2 (*A*) and the co-localization of LC3 with LAMP-2 (*B*). The scatter plots and Mander's overlap coefficient (*r*) were calculated using ImageJ. Representative images shown are typical of three experiments. *Scale bar*, 10 μm.

somes, is indicative of undamaged lysosomes/autolysosomes (Fig. 10*A*) as shown previously (69). Incubation with TAM enhanced the punctate fluorescence pattern of both Cat D and LAMP-2 and their co-localization ($r = 0.944$) in the merge relative to the control (Fig. 10*A*). This observation is again consistent with an increased number of undamaged lysosomes/autolysosomes as observed previously in TAM-incubated cells stained with acridine orange (Fig. 9*A*).

Conversely, the decreased co-localization ($r = 0.684$) and the more diffuse staining of Cat D and LAMP-2 upon incubation with Dp44mT (Fig. 10*A*) suggests that Cat D was released from damaged lysosomes. This observation also agrees with the loss

of red granular staining and increase in green cytosolic/nuclear fluorescence consistent with LMP when the cells were stained with acridine orange and incubated with Dp44mT (Fig. 9*A*). The loss of lysosomes will prevent the formation of autolysosomes and will inhibit autophagic degradation, which is in good agreement with the studies demonstrating accumulation of p62 in Dp44mT-treated cells (Fig. 4, *B* and *C*). As shown in the earlier acridine orange staining studies and in contrast to Dp44mT (Fig. 9*A*), DFO did not induce characteristics indicative of LMP. In fact, a distinct "pinpoint" punctate pattern of Cat D and LAMP-2 was observed ($r = 0.832$; Fig. 10*A*) after incubation with DFO, demonstrating that the chelator had not induced LMP.

The association of autophagosomes and lysosomes was also examined through immunofluorescence studies by observing the distribution of LC3 and LAMP-2, which are expressed in the membranes of autophagosomes and lysosomes, respectively (49, 50, 70). In control cells, weak and diffuse LC3 staining was observed together with perinuclear LAMP-2 staining that did not distinctly co-localize in the merged image ($r = 0.182$; Fig. 10*B*). After a 24-h incubation, TAM markedly enhanced the punctate formation of both LC3 and LAMP-2, leading to pronounced co-localization (*yellow*) in the merged image that was confirmed by the scatter plots and Mander's overlap coefficient ($r = 0.955$; Fig. 10*B*). This observation suggested the interaction of autophagosomes and lysosomes to form autolysosomes (71). However, the increase in LC3-II levels by TAM was shown in Fig. 2, *B* and *C*, to be due to its inhibitory effect on the degradation stage of autophagy. Considering this, the accumulation of LAMP-2-lysosomal staining along with the LC3-stained autophagosomes (Fig. 10*B*) suggests that a defect in the subsequent autophagic degradation led to increased LC3-II. Incubation with Dp44mT enhanced LC3 but not LAMP-2 staining relative to the control, and unlike TAM, there was no marked overlap in the merged image ($r = 0.530$; Fig. 10*B*). This finding indicates a lack of autolysosomal formation and the accumulation of autophagosomes. The LC3 and LAMP-2 distribution did not differ markedly from the control after incubation with DFO and was without marked co-localization ($r = 0.331$; Fig. 10*B*).

Silencing the Autophagic Initiator Beclin1 or ATG5 Inhibits the Antiproliferative Activity of Dp44mT but Not DFO—Autophagy is generally described as a prosurvival mechanism that is up-regulated in response to therapeutic agents (72, 73). However, under conditions of stress, autophagy can also promote cell death due to the disruption of the late stage autophagic process (72, 73). In this study, increased LC3-II levels induced by TAM, Dp44mT, and DFO were due at least in part to inhibition of autophagosomal degradation with Dp44mT also increasing autophagosome formation (Figs. 2, *B* and *C*, and 4, *B* and *C*). Therefore, it was of interest to determine how autophagy influences the antiproliferative activity of these agents. To address this, the initiation of autophagy was inhibited by siRNA-mediated knockdown of Beclin1 or ATG5 in MCF7 cells, and then its effects on LC3-II formation and the antiproliferative activity of TAM, Dp44mT, and DFO were examined.

Successful knockdown of Beclin1 via *BECN1* siRNA was demonstrated by a significant ($p < 0.001$) decrease in Beclin1 protein relative to the negative control siRNA under all experimental conditions after 24 or 48 h (Fig. 11, *A* and *B*). No significant ($p > 0.05$) change was observed in the TAM-induced increase in LC3-II in cells transfected with *BECN1* siRNA relative to cells transfected with negative control siRNA after 24 or 48 h (Fig. 11, *A* and *B*). In contrast, after a 24- or 48-h incubation with Dp44mT, the increase in LC3-II induced by this agent in cells transfected with negative control siRNA was significantly ($p < 0.001–0.05$) suppressed in cells transfected with *BECN1* siRNA (Fig. 11, *A* and *B*). This finding is in agreement with the previous studies in Fig. 2, *B* and *C*, demonstrating that the increase in LC3-II expression after incubation with Dp44mT was due in part to the induction of autophagosome synthesis. Similar to TAM, the DFO-induced increase in LC3-II was not significantly ($p > 0.05$) suppressed by the down-regulation of Beclin1 after 24 or 48 h (Fig. 11, *A* and *B*). This observation was also in agreement with the previous studies in Fig. 2, *B* and *C*, where the increase in LC3-II after incubation with TAM or DFO was due to their inhibitory effect on the degradation stage of autophagy.

Transfection of MCF7 cells with *ATG5* siRNA resulted in a marked and significant ($p < 0.001–0.05$) decrease in ATG5 protein under all conditions after 24 or 48 h (Fig. 11, *C* and *D*). The alterations of LC3-II expression upon silencing of ATG5 after incubation with TAM, Dp44mT, or DFO followed a trend similar to that in cells transfected with *BECN1* siRNA (*cf.* Fig. 11, *A* and *B*). The TAM- or DFO-induced increase in LC3-II expression was not significantly ($p > 0.05$) altered by ATG5 silencing (Fig. 11, *C* and *D*). However, in contrast, the increase in LC3-II induced by Dp44mT in negative control siRNA-treated cells was significantly ($p < 0.001–0.05$) suppressed by ATG5 silencing after 24 or 48 h (Fig. 11, *C* and *D*). Hence, studies using both *BECN1* siRNA and *ATG5* siRNA demonstrate that the increase in LC3-II levels after incubation with Dp44mT, but not DFO, was due in part to the induction of autophagosome synthesis (Fig. 11, *A–D*).

Considering these studies above, the effect of *BECN1* siRNA and *ATG5* siRNA on cell viability was then assessed. The down-regulation of Beclin1 significantly ($p < 0.001–0.01$) reduced the cytotoxic activity of TAM or Dp44mT, whereas no significant ($p > 0.05$) change was observed after incubation with DFO after 24 or 48 h (Fig. 12*A*). This finding suggests that autophagy plays a role in TAM- and Dp44mT-induced cell death in MCF7 cells. Conversely, ATG5 silencing only led to a significant ($p < 0.001$) decrease in the cytotoxic activity of Dp44mT after 24 or 48 h (Fig. 12*B*). No significant alteration in the cytotoxic activity of TAM or DFO was observed in cells with silenced ATG5 after 24 or 48 h (Fig. 12*B*). To explain the difference between the results achieved with Beclin1 and ATG5 silencing, we speculate that ATG5 silencing was not sufficient to effectively suppress autophagy because only a small fraction of ATG5 is required to maintain autophagic function (49). Collectively, the cytotoxic activity of Dp44mT was suppressed by both *BECN1* and *ATG5* silencing after 24 or 48 h (Fig. 12, *A* and *B*). This observation indicated an important role of persistent autophagosome syn-

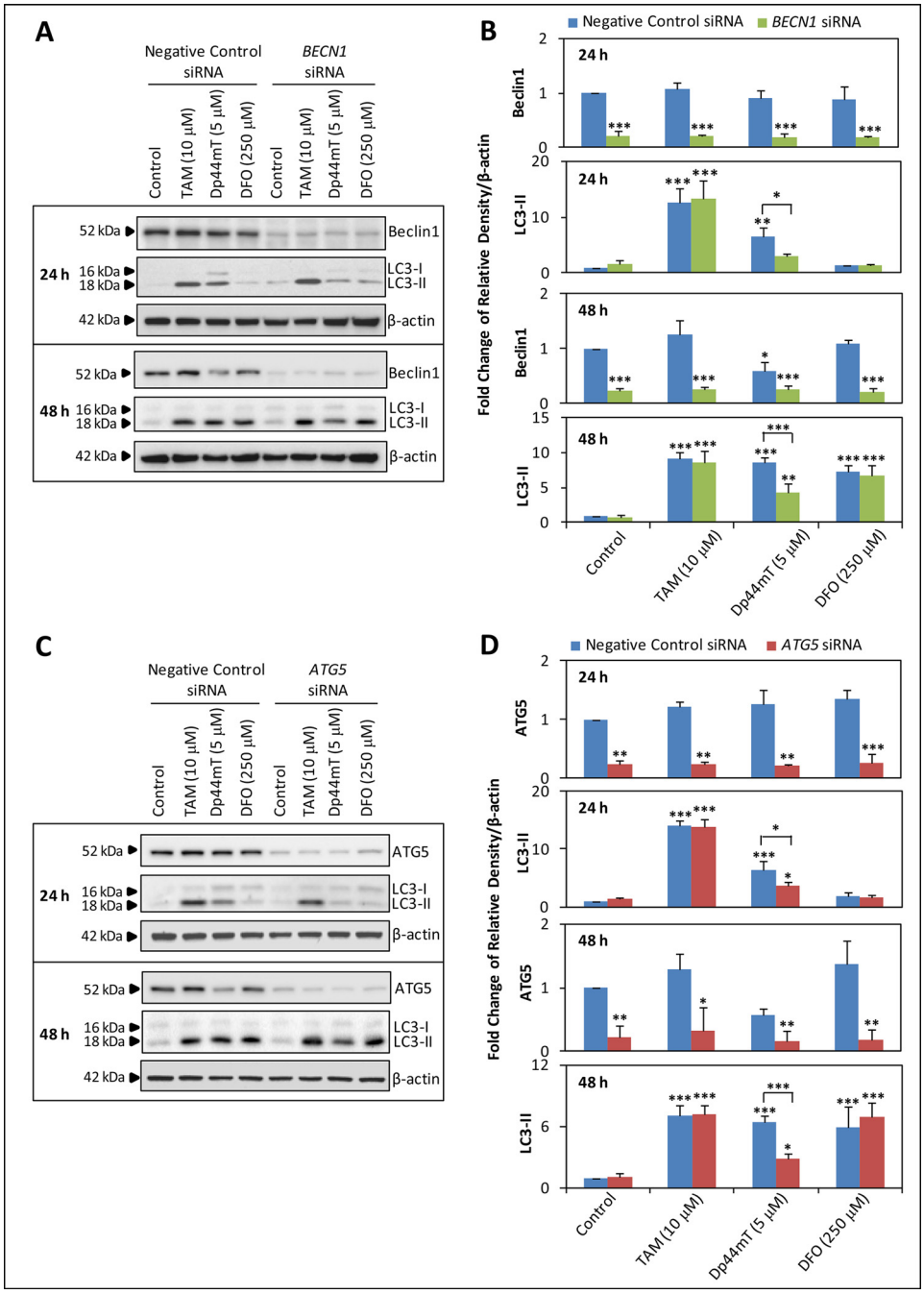

FIGURE 11. **Silencing Beclin1 (*BECN1*) or ATG5 (*ATG5*) decreases the Dp44mT-induced increase in autophagy.** *A*, MCF7 cells transfected with negative control siRNA or *BECN1* siRNA were incubated with control medium or medium containing TAM (10 μM), Dp44mT (5 μM), or DFO (250 μM) for 24 or 48 h at 37 °C. Western blotting was performed to examine Beclin1 and LC3-I/II expression. *B*, densitometric analysis (arbitrary units) of the results in *A*. *C*, MCF7 cells transfected with negative control siRNA or *ATG5* siRNA were incubated in the same conditions as in *A*. Western blotting was performed to examine ATG5 and LC3-I/II expression. *D*, densitometric analysis (arbitrary units) of the results in *C*. The representative Western blot from each study shown is typical of three experiments. Densitometric analysis is the mean of three experiments with *error bars* representing S.D. *, $p < 0.05$; **, $p < 0.01$; ***, $p < 0.001$ *versus* the control or between treatments as indicated.

thesis in the inhibition of growth and the induction of cell death mediated by Dp44mT.

Dp44mT-induced Apoptosis Is Dependent on Autophagy—Autophagy occurs in close relation to apoptosis with the existence of a "molecular switch" between these two processes (74). Dp44mT has been well characterized to inhibit proliferation by inducing cell death by apoptosis, and this occurs via lysosomal membrane permeabilization (20, 27, 75). In fact, Dp44mT induces apoptosis *in vitro* and *in vivo* with this mechanism of cell death occurring via the mitochondrial pathway where decreased Bcl-2 and increased Bax expression occur along with holocytochrome *c* release and caspase 3, 8, and 9 activation (20).

To further explore the role of autophagy in Dp44mT-induced cell death, we determined whether autophagy contributes to Dp44mT-induced apoptosis. Initially, the apoptotic cell death induced by a 24- or 48-h incubation with TAM, Dp44mT, and DFO was measured using the annexin V-FITC assay in cells preincubated with *BECN1* siRNA or *ATG5* siRNA relative to

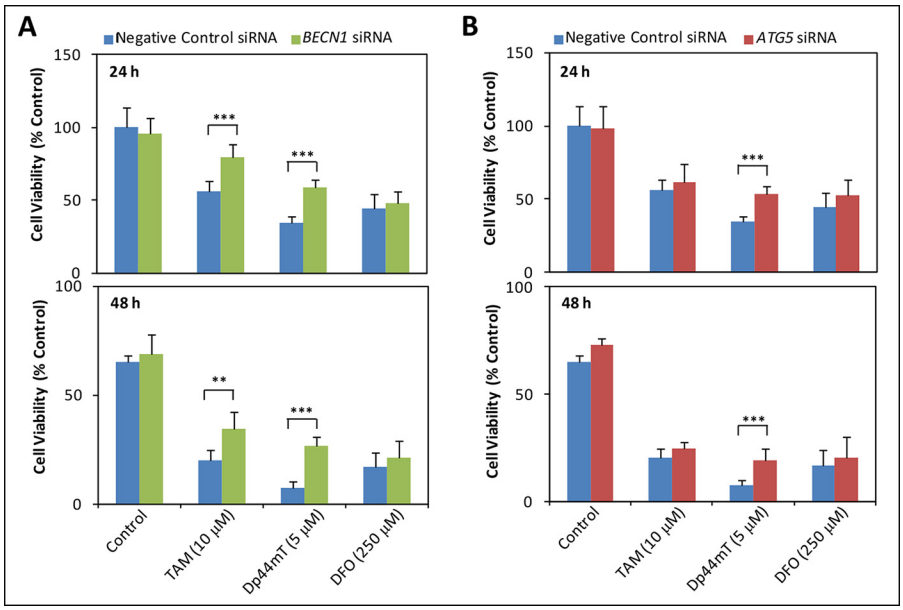

FIGURE 12. **Silencing Beclin1 (*BECN1*) or ATG5 (*ATG5*) suppresses Dp44mT-induced cell death.** *A*, cell viability of MCF7 cells transfected with negative control siRNA or *BECN1* siRNA incubated with control medium or medium containing TAM (10 μM), Dp44mT (5 μM), or DFO (250 μM) for 24 or 48 h at 37 °C. *B*, cell viability of MCF7 cells transfected with negative control siRNA or *ATG5* siRNA that were incubated under the same conditions as in *A*. Results in *A* and *B* are the mean of three experiments with *error bars* representing S.D. **, $p < 0.01$; ***, $p < 0.001$ *versus* the control or between treatments as indicated.

the negative control siRNA (Fig. 13, *A* and *B*). Comparing the efficacy of the agents at inducing apoptosis in the negative control siRNA-treated cells, it was evident that TAM and particularly Dp44mT significantly ($p < 0.001–0.01$) increased apoptosis relative to the control with Dp44mT being more active than TAM after 24 or 48 h (Fig. 13, *A* and *B*). DFO significantly ($p < 0.001$) induced apoptosis in negative control siRNA-treated cells only after 48 h (Fig. 13, *A* and *B*). No significant alteration of annexin V staining was observed for all agents after 24 or 48 h when autophagy was inhibited using *BECN1* siRNA or *ATG5* siRNA (Fig. 13, *A* and *B*).

We then assessed the expression of the antiapoptotic protein Bcl-2 and proapoptotic protein Bax by Western blotting to investigate apoptosis after a 24- or 48-h incubation with TAM, Dp44mT, or DFO in MCF7 cells where Beclin1 or ATG5 was silenced (Fig. 13, *C–F*). In these studies, the Bax:Bcl-2 ratio was calculated as it determines the vulnerability of cells to apoptosis (76). First, assessing cells transfected with negative control siRNA, only Dp44mT significantly ($p < 0.01$) increased the Bax:Bcl-2 ratio relative to the control after 24 or 48 h (Fig. 13, *C–F*) in good agreement with its effect reported previously (20). Examining cells transfected with *BECN1* siRNA, the Bax:Bcl-2 ratio was significantly ($p < 0.001$) decreased in control cells transfected with *BECN1* siRNA relative to control cells transfected with negative control siRNA after 24 h (Fig. 13, *C* and *D*). This was predominantly due to the marked and significant ($p < 0.001$) up-regulation of Bcl-2 expression, which under different conditions has been reported to have an antiautophagic function where it inhibits Beclin1 (74, 77, 78). The Bax:Bcl-2 ratio was significantly ($p < 0.01$) decreased in *BECN1* siRNA-transfected cells incubated with TAM or Dp44mT relative to negative control siRNA-transfected cells after 24 h, whereas no alteration was observed in cells incubated with DFO (Fig. 13, *C* and *D*). After 48 h, no significant alterations of the Bax:Bcl-2 ratio was observed for TAM or DFO, whereas a slight decrease was observed for Dp44mT in *BECN1* siRNA-transfected cells relative to negative control siRNA-transfected cells (Fig. 13, *C* and *D*).

Similar to the results observed with *BECN1* siRNA (Fig. 13, *C* and *D*), the Bax:Bcl-2 ratio was slightly, but not significantly, decreased in control cells transfected with *ATG5* siRNA relative to control cells transfected with negative control siRNA after 24 h (Fig. 13, *E* and *F*). Again its notable that ATG5 silencing was not sufficient to effectively suppress autophagy because only a small fraction of ATG5 is required to maintain the function of this process (49). Relative to negative control siRNA-transfected cells, TAM or DFO did not induce any significant ($p > 0.05$) change in the Bax:Bcl-2 ratio in *ATG5* siRNA-transfected cells after 24 or 48 h (Fig. 13, *E* and *F*). However, similarly to *BECN1* siRNA-transfected cells, the Bax:Bcl-2 ratio was significantly ($p < 0.05$) decreased by Dp44mT in *ATG5* siRNA-transfected cells relative to negative control siRNA-transfected cells after 24 h, and a slight decrease was observed after 48 h (Fig. 13, *E* and *F*).

Collectively, using either *BECN1* or *ATG5* siRNA, these experiments indicated that inhibition of autophagy significantly decreased Dp44mT-induced apoptosis. Considering the previous results where the antiproliferative activity of Dp44mT was also significantly reduced in cells in which autophagy was inhibited using *BECN1* or *ATG5* siRNA (Fig. 12, *A* and *B*), the decreased apoptosis is also important for explaining these data.

DISCUSSION

Considering that autophagy plays a prosurvival role in resistance against anticancer agents, this study investigated the effect of Dp44mT on autophagy (1, 4). Targeted knockdown of genes essential for autophagy such as *ATG5* and *BECN1* or by using autophagy inhibitors such as Baf A1, etc. have been shown to

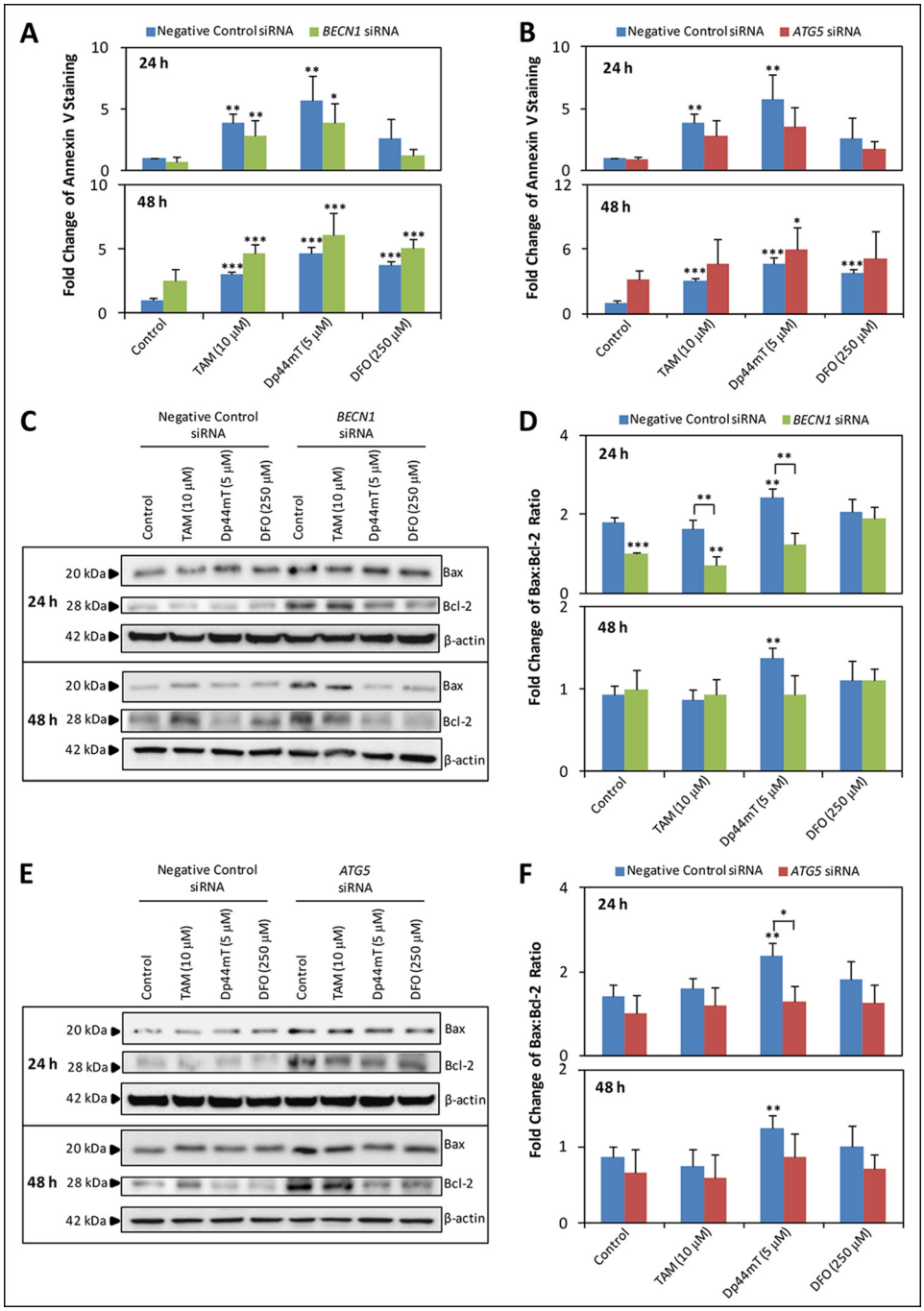

FIGURE 13. **Inhibition of autophagy initiation by silencing Beclin1 or ATG5 suppresses apoptosis induced by Dp44mT.** *A*, MCF7 cells transfected with negative control siRNA or *BECN1* siRNA were incubated with control medium or medium containing TAM (10 μM), Dp44mT (5 μM), or DFO (250 μM) for 24 or 48 h at 37 °C. The occurrence of apoptosis was examined via annexin V-FITC staining, which was quantified by flow cytometry. *B*, MCF7 cells transfected with negative control siRNA or *ATG5* siRNA that were incubated under the same conditions as in *A*. The occurrence of apoptosis was examined via annexin V-FITC staining, which was quantified by flow cytometry. *C*, MCF7 cells transfected with negative control siRNA or *BECN1* siRNA that were incubated under the same conditions as in *A*. Western blotting was performed to investigate the alteration of Bax and Bcl-2 expression. *D*, densitometric analysis (arbitrary units) of Bax and Bcl-2 in *C* is shown as the Bax:Bcl-2 ratio. *E*, MCF7 cells transfected with negative control siRNA or *ATG5* siRNA that were incubated under the same conditions as in *B*. Western blotting was performed to investigate the alteration of Bax and Bcl-2 expression. *F*, densitometric analysis (arbitrary units) of Bax and Bcl-2 in *E* is shown as the Bax:Bcl-2 ratio. Analysis of annexin V staining is the mean of three experiments with *error bars* representing S.D. The representative Western blot from each study shown is typical of three experiments. Densitometric analysis is the mean of three experiments with *error bars* representing S.D.. *, $p < 0.05$; **, $p < 0.01$; ***, $p < 0.001$ *versus* the control or between treatments as indicated.

resensitize resistant cancer cells to anticancer therapy (31–34). Moreover, this was of interest because Dp44mT can overcome drug resistance (21), and inhibition of autophagy in resistant cancer cells has been suggested as an approach to cancer eradication (4). In the present study, we have shown a mechanism whereby Dp44mT overcomes the prosurvival activity of autophagy and turns autophagy into a potentiated mechanism of cytotoxicity.

Autophagy is a dynamic, multistep process in which the accumulation of autophagosomes could indicate either

increased autophagic flux or aberrant autophagy (49, 50). Here we demonstrated an early initiation of effective autophagy upon Dp44mT treatment in studies utilizing Baf A1 to examine autophagic flux (Fig. 2, *B* and *C*). However, Dp44mT was also found to reduce autophagic clearance as indicated by p62 accumulation (Fig. 3, *B* and *C*). This was due to lysosomal permeabilization by Dp44mT (Figs. 9*A* and 10*A*), which impairs autophagosome-lysosome fusion and thus inhibits the completion of the autophagic process. To decipher the mechanism in which Dp44mT affects autophagy, the non-redox-active iron chelator DFO (14) was used in a relative comparison with Dp44mT, which forms redox-active complexes (25). DFO was found to induce an accumulation of autophagosomes by not increasing their synthesis but by inhibiting degradation of these organelles (Fig. 2, *B* and *C*).

Because iron is believed to be liberated from iron-containing proteins by autophagy (6–8), one would expect that cells deprived of iron would up-regulate autophagy to release iron stored in proteins to then be utilized by the cell (5). This would occur at an accelerated rate during the cellular iron depletion that occurs due to iron chelation. Indeed, it has been reported that ferritin delivery to lysosomes is increased in iron-depleted cells (79). It was shown that DFO induces ferritin degradation in lysosomes through induction of autophagy (80). However, in this study, DFO was not found to induce autophagy but instead inhibited autophagosome degradation (Figs. 2, *B* and *C*, and 4, *B* and *C*). Because of the poor membrane permeability of DFO, the chelator is probably taken up by fluid phase pinocytosis (81) and then incorporated into lysosomes during the endosomal-lysosomal maturation process (81–83). DFO has been reported to act as a weak base possessing lysosomotropic properties (84) that then alters the pH of the lysosomal compartment and decreases Cat D activity (85). This may explain the inhibition of autophagosome degradation observed when the cells were incubated with DFO (Figs. 2, *B* and *C*, and 4, *B* and *C*) as an acidic pH is required for lysosomal hydrolase activity and its catabolic efficiency (86).

Previous reports have suggested that TAM may increase autophagy flux under defined conditions (87, 88). However, in this investigation, the results assessing autophagic flux via the use of Baf A1 (Fig. 2, *B* and *C*) and p62 accumulation (Fig. 4, *B* and *C*) together show that the TAM-induced increase in LC3-II was due to inhibited autophagosomal degradation. This distinction between the current and previous studies may be explained by the differences in experimental conditions utilized. For instance, in the current study, MCF7 cells were grown in the presence of estrogen, whereas in previous studies, these cells were grown in the absence of estrogen, which would enable effective binding of TAM to the estrogen receptor (87, 88). It is known that estradiol inhibits cell death induced by TAM (88). Moreover, studies have reported numerous pharmacological effects of TAM that are independent of the estrogen receptor such as its ability to inhibit the acidification of lysosomes (89, 90) and induce LMP (91). These effects of TAM ultimately lead to the impairment of lysosomal function and reduction of autophagosome clearance and may explain the decrease in autophagosome degradation observed after incubation with this agent (Figs. 2, *B* and *C*, and 4, *B* and *C*). Considering this, it is notable that despite one of the cell lines used herein being classically referred to as estrogen receptor-negative (*i.e.* MDA-MB-231) recent reassessment has actually demonstrated that it expresses the estrogen receptor (92). Hence, the observed effects of TAM on autophagy in breast cancer cells (Fig. 6) could be dependent or independent of the estrogen receptor.

The ability of Dp44mT to induce autophagy was found to be dependent on its redox activity upon binding metals (Fig. 7, *A–D*). In agreement with this observation, co-incubation with the glutathione precursor NAC prevented the Dp44mT-induced increase in autophagic flux (Fig. 8, *A–D*). There is a growing body of evidence showing that autophagy is activated by ROS as a cytoprotective process in which ROS production is increased and is required for induction of autophagy under starvation conditions (93). One of the classical targets of ROS is lysosomes where oxidizing conditions lead to lysosomal membrane destabilization and thereby promote the leakage of hydrolytic enzymes to induce further cellular damage (29, 65). The redox activity of Dp44mT is the culprit causing LMP as co-incubation with NAC inhibited the Dp44mT-induced increase of the mean green:red fluorescence ratio in acridine orange staining (Fig. 9*B*). The LMP caused by Dp44mT has been shown to induce apoptosis, which ultimately leads to cell death (27).

Because the effect of redox stress induced by Dp44mT on lysosomes is lethal, it is of interest to consider whether the increase in autophagosome synthesis by Dp44mT is a cell survival response as observed in classical autophagy or whether it actually enhances cell death by this agent. The dual role of redox activity by Dp44mT in autophagy may be explained by the opposing roles of the lysosomal system under an oxidizing environment (35, 94). Under oxidizing conditions leading to cellular damage, the lysosomal membrane is destabilized, leading to leakage of the hydrolase enzymes into the cytosol (35, 94). The magnitude of the cellular damage varies with the intensity of the oxidative stress, which determines the degree of disruption of the lysosomal membrane (35, 94). It was hypothesized by Kiffin *et al.* (94) that moderate oxidative stress affecting only a small percentage of lysosomes may activate autophagy to sequester "leaking" lysosomes out from the cytosol. This may explain the increase in autophagic flux after incubation with Dp44mT where in the first stages of oxidative injury the lysosomal system plays a protective role and eliminates damaged intracellular components through autophagy.

Conversely, during intense acute oxidative stress, the lack of a significant number of functional lysosomes left after the cellular insult could prevent the removal of the damaged lysosomes (35, 94). The reduced number of lysosomes would then result in a decrease in autophagosome degradation (94). This scenario would explain the observed p62 accumulation induced by Dp44mT (Fig. 4, *B* and *C*). In this case, p62 could not be degraded by the functional autolysosomes as the lysosomes responsible for their formation had been damaged or destroyed (Fig. 4, *B* and *C*).

The effect of Dp44mT to disturb the balance between autophagosome production and autophagosome degradation in this study may transform generally protective autophagy into

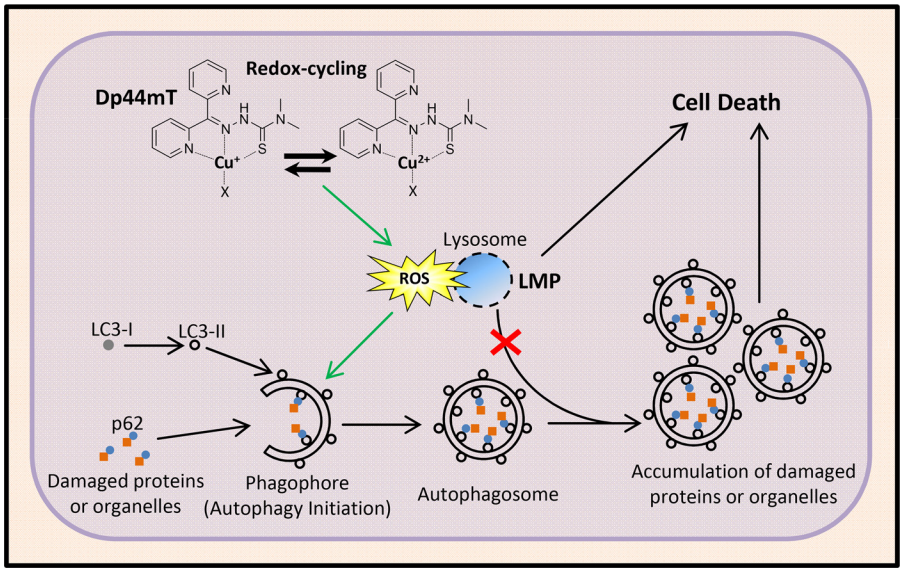

FIGURE 14. **Schematic demonstrating the effects of Dp44mT in converting autophagy into a cell death process through the 1) simultaneous induction of autophagy to increase autophagosome synthesis and 2) prevention of autophagosome degradation as an autolysosome by damaging lysosomal integrity.** The latter has been shown to be due to the ability of Dp44mT to form redox-active copper complexes that redox cycle to generate ROS that induce LMP (27). The loss of integrity to the lysosome results in the release of its contents, which can induce apoptosis, into the cytosol (27). The resulting accumulation of autophagosomes from these two mechanisms leads to a buildup of damaged proteins and organelles, which provokes cell death in addition to LMP-induced apoptosis.

"destructive autophagy." If autophagy is activated when the cell is under intense stress but is insufficient for the removal of the cellular debris due to damage to the lysosomal compartment, the intracellular levels of death factors (*e.g.* death-associated protein kinase and the tumor necrosis factor-related apoptosis-inducing ligand) (64) would increase to activate apoptosis and cell death (5, 35, 94). Along with its ability to up-regulate autophagy, Dp44mT was observed to destabilize the lysosomal membrane, leading to the release of hydrolytic enzymes such as Cat D into the cytoplasm (Fig. 10*A*). As shown previously, targeting lysosomal integrity plays a key role in the antiproliferative activity of Dp44mT (27). Thus, the effect of Dp44mT in inducing autophagy may be detrimental to the cell when this effect is coupled with LMP. Moreover, the fact that the inhibition of autophagy by *BECN1* and *ATG5* silencing abrogated cell death induced by Dp44mT (Fig. 12, *A* and *B*) indicates that the early induction of autophagy contributes to the execution of cell death by this agent. In this regard, our study adds to the increasing evidence that persistent autophagy in response to cellular stress serves as a potent death signal.

Autophagic cell death can occur in collaboration with apoptosis or as a backup mechanism when apoptosis is defective (95, 96). Studies have reported that cytotoxic drugs can induce autophagic cell death when the apoptotic pathway is non-functional (32, 37). In this study, Dp44mT was found to induce classical markers of both autophagy (Fig. 2, *B* and *C*) and apoptosis (Fig. 13). The coincidence of apoptosis and autophagy has also been observed in MCF7 cells treated with the DNA topoisomerase I inhibitor camptothecin where autophagic cell death was found to be complementary to apoptosis in eliminating the remaining, more resistant cells (97). Several investigations have suggested that the co-existence of apoptotic and non-apoptotic modes of cell death is a consequence of the intracytoplasmic release of lysosomal enzymes such as cathepsins, which are involved in caspase-dependent and -independent cell death (36, 97). Studies have also reported autophagy to be essential for caspase-dependent cell death and that it appears to act upstream of apoptosis (98, 99). Clearly, identifying the key mediators in the occurrence of both autophagic and apoptotic cell death by Dp44mT warrants further investigation.

In conclusion, this study identified the ability of Dp44mT to convert autophagy into a cell death process through the 1) induction of autophagy to increase autophagosome synthesis and 2) prevention of autophagosome degradation as an autolysosome by damaging lysosomal integrity (Fig. 14). The resulting accumulation of autophagosomes leads to a buildup of cellular debris such as protein aggregates and damaged organelles, which are lethal to the cell (Fig. 14). This effect potentiates the cell death caused by Dp44mT through LMP-induced apoptosis (Fig. 10). Hence, Dp44mT was able to overcome the prosurvival activity of autophagy and actually utilize the autophagic machinery to induce cancer cell death.

REFERENCES

1. Kondo, Y., Kanzawa, T., Sawaya, R., and Kondo, S. (2005) The role of autophagy in cancer development and response to therapy. *Nat. Rev. Cancer* **5,** 726–734
2. Kroemer, G., and Jäättelä, M. (2005) Lysosomes and autophagy in cell death control. *Nat. Rev. Cancer* **5,** 886–897
3. Lum, J. J., DeBerardinis, R. J., Thompson, C. B. (2005) Autophagy in metazoans: cell survival in the land of plenty. *Nat. Rev. Mol. Cell Biol.* **6,** 439–448
4. Mathew, R., Karantza-Wadsworth, V., and White, E. (2007) Role of autophagy in cancer. *Nat. Rev. Cancer* **7,** 961–967
5. Kurz, T., Terman, A., Gustafsson, B., and Brunk, U. (2008) Lysosomes in iron metabolism, ageing and apoptosis. *Histochem. Cell Biol.* **129,** 389–406
6. Yu, Z., Persson, H. L., Eaton, J. W., and Brunk, U. T. (2003) Intralysosomal iron: a major determinant of oxidant-induced cell death. *Free Radic. Biol. Med.* **34,** 1243–1252

7. Persson, H. L., Yu, Z., Tirosh, O., Eaton, J. W., and Brunk, U. T. (2003) Prevention of oxidant-induced cell death by lysosomotropic iron chelators. *Free Radic. Biol. Med.* **34,** 1295–1305
8. Kurz, T., Leake, A., Von Zglinicki, T., and Brunk, U. T. (2004) Relocalized redox-active lysosomal iron is an important mediator of oxidative-stress-induced DNA damage. *Biochem. J.* **378,** 1039–1045
9. Kalinowski, D. S., and Richardson, D. R. (2005) The evolution of iron chelators for the treatment of iron overload disease and cancer. *Pharmacol. Rev.* **57,** 547–583
10. Buss, J. L., Greene, B. T., Turner, J., Torti, F. M., and Torti, S. V. (2004) Iron chelators in cancer chemotherapy. *Curr. Top. Med. Chem.* **4,** 1623–1635
11. Le, N. T., and Richardson, D. R. (2002) The role of iron in cell cycle progression and the proliferation of neoplastic cells. *Biochim. Biophys. Acta* **1603,** 31–46
12. Buss, J. L., Torti, F. M., and Torti, S. V. (2003) The role of iron chelation in cancer therapy. *Curr. Med. Chem.* **10,** 1021–1034
13. Blatt, J., and Stitely, S. (1987) Antineuroblastoma activity of desferoxamine in human cell lines. *Cancer Res.* **47,** 1749–1750
14. Chaston, T. B., Lovejoy, D. B., Watts, R. N., and Richardson, D. R. (2003) Examination of the antiproliferative activity of iron chelators: multiple cellular targets and the different mechanism of action of triapine compared with desferrioxamine and the potent pyridoxal isonicotinoyl hydrazone analogue 311. *Clin. Cancer Res.* **9,** 402–414
15. Donfrancesco, A., Deb, G., Dominici, C., Pileggi, D., Castello, M. A., and Helson, L. (1990) Effects of a single course of deferoxamine in neuroblastoma patients. *Cancer Res.* **50,** 4929–4930
16. Donfrancesco, A., Deb, G., Dominici, C., Angioni, A., Caniglia, M., De Sio, L., Fidani, P., Amici, A., and Helson, L. (1992) Deferoxamine, cyclophosphamide, etoposide, carboplatin, and thiotepa (D-CECaT): a new cytoreductive chelation-chemotherapy regimen in patients with advanced neuroblastoma. *Am. J. Clin. Oncol.* **15,** 319–322
17. Estrov, Z., Tawa, A., Wang, X. H., Dubé, I. D., Sulh, H., Cohen, A., Gelfand, E. W., and Freedman, M. H. (1987) *In vitro* and *in vivo* effects of deferoxamine in neonatal acute leukemia. *Blood* **69,** 757–761
18. Selig, R. A., Madafiglio, J., Haber, M., Norris, M. D., White, L., and Stewart, B. W. (1993) Ferritin production and desferrioxamine cytotoxicity in human neuroblastoma cell lines. *Anticancer Res.* **13,** 721–725
19. Richardson, D., Ponka, P., and Baker, E. (1994) The effect of the iron(III) chelator, desferrioxamine, on iron and transferrin uptake by the human malignant melanoma cell. *Cancer Res.* **54,** 685–689
20. Yuan, J., Lovejoy, D. B., and Richardson, D. R. (2004) Novel di-2-pyridyl derived iron chelators with marked and selective antitumor activity: *in vitro* and *in vivo* assessment. *Blood* **104,** 1450–1458
21. Whitnall, M., Howard, J., Ponka, P., and Richardson, D. R. (2006) A class of iron chelators with a wide spectrum of potent antitumor activity that overcomes resistance to chemotherapeutics. *Proc. Natl. Acad. Sci. U.S.A.* **103,** 14901–14906
22. Rao, V. A., Klein, S. R., Agama, K. K., Toyoda, E., Adachi, N., Pommier, Y., and Shacter, E. B. (2009) The iron chelator Dp44mT causes DNA damage and selective inhibition of topoisomerase IIα in breast cancer cells. *Cancer Res.* **69,** 948–957
23. Rao, V. A., Zhang, J., Klein, S. R., Espandiari, P., Knapton, A., Dickey, J. S., Herman, E., and Shacter, E. B. (2011) The iron chelator Dp44mT inhibits the proliferation of cancer cells but fails to protect from doxorubicin-induced cardiotoxicity in spontaneously hypertensive rats. *Cancer Chemother. Pharmacol.* **68,** 1125–1134
24. Liu, W., Xing, F., Iiizumi-Gairani, M., Okuda, H., Watabe, M., Pai, S. K., Pandey, P. R., Hirota, S., Kobayashi, A., Mo, Y.-Y., Fukuda, K., Li, Y., and Watabe, K. (2012) N-myc downstream regulated gene 1 modulates Wnt-β-catenin signalling and pleiotropically suppresses metastasis. *EMBO Mol. Med.* **4,** 93–108
25. Jansson, P. J., Sharpe, P. C., Bernhardt, P. V., and Richardson, D. R. (2010) Novel thiosemicarbazones of the ApT and DpT Series and their copper complexes: identification of pronounced redox activity and characterization of their antitumor activity. *J. Med. Chem.* **53,** 5759–5769
26. Lovejoy, D. B., Sharp, D. M., Seebacher, N., Obeidy, P., Prichard, T., Stefani, C., Basha, M. T., Sharpe, P. C., Jansson, P. J., Kalinowski, D. S., Bernhardt, P. V., and Richardson, D. R. (2012) Novel second-generation di-2-pyridylketone thiosemicarbazones show synergism with standard chemotherapeutics and demonstrate potent activity against lung cancer xenografts after oral and intravenous administration *in vivo*. *J. Med. Chem.* **55,** 7230–7244
27. Lovejoy, D. B., Jansson, P. J., Brunk, U. T., Wong, J., Ponka, P., and Richardson, D. R. (2011) Antitumor activity of metal-chelating compound Dp44mT is mediated by formation of a redox-active copper complex that accumulates in lysosomes. *Cancer Res.* **71,** 5871–5880
28. Gaál, A., Orgován, G., Polgári, Z., Réti, A., Mihucz, V. G., Bősze, S., Szoboszlai, N., and Streli, C. (2014) Complex forming competition and *in-vitro* toxicity studies on the applicability of di-2-pyridylketone-4,4,-dimethyl-3-thiosemicarbazone (Dp44mT) as a metal chelator. *J. Inorg. Biochem.* **130,** 52–58
29. Kurz, T., Gustafsson, B., and Brunk, U. T. (2006) Intralysosomal iron chelation protects against oxidative stress-induced cellular damage. *FEBS J.* **273,** 3106–3117
30. Richardson, D. R., and Milnes, K. (1997) The potential of iron chelators of the pyridoxal isonicotinoyl hydrazone class as effective antiproliferative agents II: the mechanism of action of ligands derived from salicylaldehyde benzoyl hydrazone and 2-hydroxy-1-naphthylaldehyde benzoyl hydrazone. *Blood* **89,** 3025–3038
31. Liu, D., Yang, Y., Liu, Q., and Wang, J. (2011) Inhibition of autophagy by 3-MA potentiates cisplatin-induced apoptosis in esophageal squamous cell carcinoma cells. *Med. Oncol.* **28,** 105–111
32. Voss, V., Senft, C., Lang, V., Ronellenfitsch, M. W., Steinbach, J. P., Seifert, V., and Kögel, D. (2010) The pan-Bcl-2 Inhibitor (−)-gossypol triggers autophagic cell death in malignant glioma. *Mol. Cancer Res.* **8,** 1002–1016
33. Kanzawa, T., Germano, I. M., Komata, T., Ito, H., Kondo, Y., and Kondo, S. (2004) Role of autophagy in temozolomide-induced cytotoxicity for malignant glioma cells. *Cell Death Differ.* **11,** 448–457
34. Bellodi, C., Lidonnici, M. R., Hamilton, A., Helgason, G. V., Soliera, A. R., Ronchetti, M., Galavotti, S., Young, K. W., Selmi, T., Yacobi, R., Van Etten, R. A., Donato, N., Hunter, A., Dinsdale, D., Tirrò, E., Vigneri, P., Nicotera, P., Dyer, M. J., Holyoake, T., Salomoni, P., and Calabretta, B. (2009) Targeting autophagy potentiates tyrosine kinase inhibitor-induced cell death in Philadelphia chromosome-positive cells, including primary CML stem cells. *J. Clin. Investig.* **119,** 1109–1123
35. Chen, Y., McMillan-Ward, E., Kong, J., Israels, S. J., and Gibson, S. B. (2008) Oxidative stress induces autophagic cell death independent of apoptosis in transformed and cancer cells. *Cell Death Differ.* **15,** 171–182
36. Gonzalez, P., Mader, I., Tchoghandjian, A., Enzenmüller, S., Cristofanon, S., Basit, F., Debatin, K.-M., and Fulda, S. (2012) Impairment of lysosomal integrity by B10, a glycosylated derivative of betulinic acid, leads to lysosomal cell death and converts autophagy into a detrimental process. *Cell Death Differ.* **19,** 1337–1346
37. Wong, V. K., Li, T., Law, B. Y., Ma, E. D., Yip, N. C., Michelangeli, F., Law, C. K., Zhang, M. M., Lam, K. Y., Chan, P. L., and Liu, L. (2013) Saikosaponin-d, a novel SERCA inhibitor, induces autophagic cell death in apoptosis-defective cells. *Cell Death Dis.* **4,** e720
38. Shimizu, S., Kanaseki, T., Mizushima, N., Mizuta, T., Arakawa-Kobayashi, S., Thompson, C. B., and Tsujimoto, Y. (2004) Role of Bcl-2 family proteins in a non-apoptotic programmed cell death dependent on autophagy genes. *Nat. Cell Biol.* **6,** 1221–1228
39. Richardson, D. R., Sharpe, P. C., Lovejoy, D. B., Senaratne, D., Kalinowski, D. S., Islam, M., and Bernhardt, P. V. (2006) Dipyridyl thiosemicarbazone chelators with potent and selective antitumor activity form iron complexes with redox activity. *J. Med. Chem.* **49,** 6510–6521
40. Kalinowski, D. S., Sharpe, P. C., Bernhardt, P. V., and Richardson, D. R. (2007) Design, synthesis, and characterization of new iron chelators with anti-proliferative activity: structure-activity relationships of novel thiohydrazone analogues. *J. Med. Chem.* **50,** 6212–6225
41. Richardson, D. R., Tran, E. H., and Ponka, P. (1995) The potential of iron chelators of the pyridoxal isonicotinoyl hydrazone class as effective antiproliferative agents. *Blood* **86,** 4295–4306
42. Gao, J., and Richardson, D. R. (2001) The potential of iron chelators of the pyridoxal isonicotinoyl hydrazone class as effective antiproliferative agents, IV: the mechanisms involved in inhibiting cell-cycle progression. *Blood* **98,** 842–850

43. Le, N. T., and Richardson, D. R. (2004) Iron chelators with high antiproliferative activity up-regulate the expression of a growth inhibitory and metastasis suppressor gene: a link between iron metabolism and proliferation. *Blood* **104,** 2967–2975
44. Chen, Z., Zhang, D., Yue, F., Zheng, M., Kovacevic, Z., and Richardson, D. R. (2012) The iron chelators Dp44mT and DFO inhibit TGFβ-induced epithelial-mesenchymal transition via up-regulation of N-myc downstream-regulated gene 1 (NDRG1). *J. Biol. Chem.* **287,** 17016–17028
45. Esteve, J. M., and Knecht, E. (2011) Mechanisms of autophagy and apoptosis: recent developments in breast cancer cells. *World J. Biol. Chem.* **2,** 232–238
46. Samaddar, J. S., Gaddy, V. T., Duplantier, J., Thandavan, S. P., Shah, M., Smith, M. J., Browning, D., Rawson, J., Smith, S. B., Barrett, J. T., and Schoenlein, P. V. (2008) A role for macroautophagy in protection against 4-hydroxytamoxifen-induced cell death and the development of antiestrogen resistance. *Mol. Cancer Ther.* **7,** 2977–2987
47. Schoenlein, P. V., Periyasamy-Thandavan, S., Samaddar, J. S., Jackson, W. H., and Barrett, J. T. (2009) Autophagy facilitates the progression of ERα-positive breast cancer cells to antiestrogen resistance. *Autophagy* **5,** 400–403
48. Brooks, S. C., Locke, E. R., and Soule, H. D. (1973) Estrogen receptor in a human cell line (MCF-7) from breast carcinoma. *J. Biol. Chem.* **248,** 6251–6253
49. Mizushima, N., Yoshimori, T., and Levine, B. (2010) Methods in mammalian autophagy research. *Cell* **140,** 313–326
50. Klionsky, D. J., Abdalla, F. C., Abeliovich, H., Abraham, R. T., Acevedo-Arozena, A., Adeli, K., Agholme, L., Agnello, M., Agostinis, P., and Aguirre-Ghiso, J. A. (2012) Guidelines for the use and interpretation of assays for monitoring autophagy. *Autophagy* **8,** 445–544
51. Yang, Z. J., Chee, C. E., Huang, S., and Sinicrope, F. A. (2011) The role of autophagy in cancer: therapeutic implications. *Mol. Cancer Ther.* **10,** 1533–1541
52. Quach, P., Gutierrez, E., Basha, M. T., Kalinowski, D. S., Sharpe, P. C., Lovejoy, D. B., Bernhardt, P. V., Jansson, P. J., and Richardson, D. R. (2012) Methemoglobin formation by triapine, di-2-pyridylketone-4,4-dimethyl-3-thiosemicarbazone (Dp44mT), and other anticancer thiosemicarbazones: identification of novel thiosemicarbazones and therapeutics that prevent this effect. *Mol. Pharmacol.* **82,** 105–114
53. Yamamoto, A., Tagawa, Y., Yoshimori, T., Moriyama, Y., Masaki, R., and Tashiro, Y. (1998) Bafilomycin A1 prevents maturation of autophagic vacuoles by inhibiting fusion between autophagosomes and lysosomes in rat hepatoma cell Line, H-4-II-E cells. *Cell Struct. Funct.* **23,** 33–42
54. Sahni, S., Bae, D. H., Lane, D. J., Kovacevic, Z., Kalinowski, D. S., Jansson, P. J., and Richardson, D. R. (2014) The metastasis suppressor, N-myc downstream-regulated gene 1 (NDRG1), inhibits stress-induced autophagy in cancer cells. *J. Biol. Chem.* **289,** 9692–9709
55. Bjørkøy, G., Lamark, T., Brech, A., Outzen, H., Perander, M., Overvatn, A., Stenmark, H., and Johansen, T. (2005) p62/SQSTM1 forms protein aggregates degraded by autophagy and has a protective effect on huntingtin-induced cell death. *J. Cell Biol.* **171,** 603–614
56. Puissant, A., Robert, G., Fenouille, N., Luciano, F., Cassuto, J.-P., Raynaud, S., and Auberger, P. (2010) Resveratrol promotes autophagic cell death in chronic myelogenous leukemia cells via JNK-mediated p62/SQSTM1 expression and AMPK activation. *Cancer Res.* **70,** 1042–1052
57. Robert, G., Ben Sahra, I., Puissant, A., Colosetti, P., Belhacene, N., Gounon, P., Hofman, P., Bost, F., Cassuto, J.-P., and Auberger, P. (2009) Acadesine kills chronic myelogenous leukemia (CML) cells through PKC-dependent induction of autophagic cell death. *PLoS ONE* **4,** e7889
58. Sawicki, S. G., and Godman, G. C. (1971) On the differential cytotoxicity of actinomycin D. *J. Cell Biol.* **50,** 746–761
59. Zhang, Y., Tang, Z. H., Ren, Z., Qu, S. L., Liu, M. H., Liu, L. S., and Jiang, Z. S. (2013) Hydrogen sulfide, the next potent preventive and therapeutic agent in aging and age-associated diseases. *Mol. Cell. Biol.* **33,** 1104–1113
60. Predmore, B. L., Lefer, D. J., and Gojon, G. (2012) Hydrogen sulfide in biochemistry and medicine. *Antioxid. Redox Signal.* **17,** 119–140
61. Aruoma, O. I., Halliwell, B., Hoey, B. M., and Butler, J. (1989) The antioxidant action of N-acetylcysteine: its reaction with hydrogen peroxide, hydroxyl radical, superoxide, and hypochlorous acid. *Free Radic. Biol. Med.* **6,** 593–597
62. Samuni, Y., Goldstein, S., Dean, O. M., and Berk, M. (2013) The chemistry and biological activities of N-acetylcysteine. *Biochim. Biophys. Acta* **1830,** 4117–4129
63. Yu, H., Zhou, Y., Lind, S. E., and Ding, W.-Q. (2009) Clioquinol targets zinc to lysosomes in human cancer cells. *Biochem. J.* **417,** 133–139
64. Paglin, S., Hollister, T., Delohery, T., Hackett, N., McMahill, M., Sphicas, E., Domingo, D., and Yahalom, J. (2001) A novel response of cancer cells to radiation involves autophagy and formation of acidic vesicles. *Cancer Res.* **61,** 439–444
65. Brunk, U. T., Dalen, H., Roberg, K., and Hellquist, H. B. (1997) Photooxidative disruption of lysosomal membranes causes apoptosis of cultured human fibroblasts. *Free Radic. Biol. Med.* **23,** 616–626
66. Farkas, E., Csoka, H., Micera, G., and Dessi, A. (1997) Copper(II), nickel(II), zinc(II), and molybdenum(VI) complexes of desferrioxamine B in aqueous solution. *J. Inorg. Biochem.* **65,** 281–286
67. Bolte, S., and Cordelières, F. P. (2006) A guided tour into subcellular colocalization analysis in light microscopy. *J. Microsc.* **224,** 213–232
68. Manders, E. M., Verbeek, F. J., and Aten, J. A. (1993) Measurement of co-localization of objects in dual-colour confocal images. *J. Microsc.* **169,** 375–382
69. Yelamanchili, S. V., Chaudhuri, A. D., Flynn, C. T., and Fox, H. S. (2011) Upregulation of cathepsin D in the caudate nucleus of primates with experimental parkinsonism. *Mol. Neurodegener.* **6,** 52
70. Eskelinen, E.-L. (2006) Roles of LAMP-1 and LAMP-2 in lysosome biogenesis and autophagy. *Mol. Aspects Med.* **27,** 495–502
71. Tasdemir, E., Maiuri, M. C., Galluzzi, L., Vitale, I., Djavaheri-Mergny, M., D'Amelio, M., Criollo, A., Morselli, E., Zhu, C., Harper, F., Nannmark, U., Samara, C., Pinton, P., Vicencio, J. M., Carnuccio, R., Moll, U. M., Madeo, F., Paterlini-Brechot, P., Rizzuto, R., Szabadkai, G., Pierron, G., Blomgren, K., Tavernarakis, N., Codogno, P., Cecconi, F., and Kroemer, G. (2008) Regulation of autophagy by cytoplasmic p53. *Nat. Cell Biol.* **10,** 676–687
72. Kenific, C. M., Thorburn, A., and Debnath, J. (2010) Autophagy and metastasis: another double-edged sword. *Curr. Opin. Cell Biol.* **22,** 241–245
73. White, E., and DiPaola, R. S. (2009) The double-edged sword of autophagy modulation in cancer. *Clin. Cancer Res.* **15,** 5308–5316
74. Luo, S., and Rubinsztein, D. C. (2007) Atg5 and Bcl-2 provide novel insights into the interplay between apoptosis and autophagy. *Cell Death Differ.* **14,** 1247–1250
75. Noulsri, E., Richardson, D. R., Lerdwana, S., Fucharoen, S., Yamagishi, T., Kalinowski, D. S., and Pattanapanyasat, K. (2009) Antitumor activity and mechanism of action of the iron chelator, Dp44mT, against leukemic cells. *Am. J. Hematol.* **84,** 170–176
76. Raisova, M., Hossini, A. M., Eberle, J., Riebeling, C., Wieder, T., Sturm, I., Daniel, P. T., Orfanos, C. E., and Geilen, C. C. (2001) The Bax/Bcl-2 ratio determines the susceptibility of human melanoma cells to CD95/Fas-mediated apoptosis. *J. Invest. Dermatol.* **117,** 333–340
77. Yousefi, S., Perozzo, R., Schmid, I., Ziemiecki, A., Schaffner, T., Scapozza, L., Brunner, T., and Simon, H.-U. (2006) Calpain-mediated cleavage of Atg5 switches autophagy to apoptosis. *Nat. Cell Biol.* **8,** 1124–1132
78. Pattingre, S., Tassa, A., Qu, X., Garuti, R., Liang, X. H., Mizushima, N., Packer, M., Schneider, M. D., and Levine, B. (2005) Bcl-2 antiapoptotic proteins inhibit Beclin 1-dependent autophagy. *Cell* **122,** 927–939
79. Asano, T., Komatsu, M., Yamaguchi-Iwai, Y., Ishikawa, F., Mizushima, N., and Iwai, K. (2011) Distinct mechanisms of ferritin delivery to lysosomes in iron-depleted and iron-replete cells. *Mol. Cell. Biol.* **31,** 2040–2052
80. De Domenico, I., Ward, D. M., and Kaplan, J. (2009) Specific iron chelators determine the route of ferritin degradation. *Blood* **114,** 4546–4551
81. Lloyd, J. B., Cable, H., and Rice-Evans, C. (1991) Evidence that desferrioxamine cannot enter cells by passive diffusion. *Biochem. Pharmacol.* **41,** 1361–1363
82. Doulias, P.-T., Christoforidis, S., Brunk, U. T., and Galaris, D. (2003) Endosomal and lysosomal effects of desferrioxamine: protection of HeLa cells from hydrogen peroxide-induced DNA damage and induction of cell-cycle arrest. *Free Radic. Biol. Med.* **35,** 719–728
83. Persson, H. L., and Richardson, D. R. (2005) Iron-binding drugs targeted to lysosomes: a potential strategy to treat inflammatory lung disorders. *Expert Opin. Investig. Drugs* **14,** 997–1008

84. Jeong, J., and Levine, R. L. (2006) Desferrioxamine is both an iron chelator and a lysosomotropic amine. *FASEB J.* **20,** A49
85. Dorer, F. E., Lentz, K. E., Kahn, J. R., Levine, M., and Skeggs, L. T. (1978) A comparison of the substrate specificities of cathepsin D and pseudorenin. *J. Biol. Chem.* **253,** 3140–3142
86. Cooper, G. M. (1997) Lysosomes. in *The Cell: A Molecular Approach* (Fitzgerald, P. J., and Sinauer, A. D., eds), pp. 379–384, 2nd Ed., Sinauer Associates, Sunderland, MA
87. Qadir, M. A., Kwok, B., Dragowska, W. H., To, K. H., Le, D., Bally, M. B., and Gorski, S. (2008) Macroautophagy inhibition sensitizes tamoxifen-resistant breast cancer cells and enhances mitochondrial depolarization. *Breast Cancer Res. Treat.* **112,** 389–403
88. Bursch, W., Ellinger, A., Kienzl, H., Török, L., Pandey, S., Sikorska, M., Walker, R., and Hermann, R. S. (1996) Active cell death induced by the anti-estrogens tamoxifen and ICI 164 384 in human mammary carcinoma cells (MCF-7) in culture: the role of autophagy. *Carcinogenesis* **17,** 1595–1607
89. Chen, Y., Schindler, M., and Simon, S. M. (1999) A mechanism for tamoxifen-mediated inhibition of acidification. *J. Biol. Chem.* **274,** 18364–18373
90. Altan, N., Chen, Y., Schindler, M., and Simon, S. M. (1999) Tamoxifen inhibits acidification in cells independent of the estrogen receptor. *Proc. Natl. Acad. Sci. U.S.A.* **96,** 4432–4437
91. Hwang, J. J., Kim, H. N., Kim, J., Cho, D.-H., Kim, M. J., Kim, Y.-S., Kim, Y., Park, S.-J., and Koh, J.-Y. (2010) Zinc(II) ion mediates tamoxifen-induced autophagy and cell death in MCF-7 breast cancer cell line. *BioMetals* **23,** 997–1013
92. Ford, C. H., Al-Bader, M., Al-Ayadhi, B., and Francis, I. (2011) Reassessment of estrogen receptor expression in human breast cancer cell lines. *Anticancer Res.* **31,** 521–527
93. Scherz-Shouval, R., Shvets, E., Fass, E., Shorer, H., Gil, L., and Elazar, Z. (2007) Reactive oxygen species are essential for autophagy and specifically regulate the activity of Atg4. *EMBO J.* **26,** 1749–1760
94. Kiffin, R., Bandyopadhyay, U., and Cuervo, A. M. (2006) Oxidative stress and autophagy. *Antioxid. Redox Signal.* **8,** 152–162
95. Eisenberg-Lerner, A., Bialik, S., Simon, H.-U., and Kimchi, A. (2009) Life and death partners: apoptosis, autophagy and the cross-talk between them. *Cell Death Differ.* **16,** 966–975
96. Mariño, G., Niso-Santano, M., Baehrecke, E. H., and Kroemer, G. (2014) Self-consumption: the interplay of autophagy and apoptosis. *Nat. Rev. Mol. Cell Biol.* **15,** 81–94
97. Lamparska-Przybysz, M., Gajkowska, B., and Motyl, T. (2005) Cathepsins and BID are involved in the molecular switch between apoptosis and autophagy in breast cancer MCF-7 cells exposed to camptothecin. *J. Physiol. Pharmacol.* **56,** 159–179
98. Wirawan, E., Vande Walle, L., Kersse, K., Cornelis, S., Claerhout, S., Vanoverberghe, I., Roelandt, R., De Rycke, R., Verspurten, J., Declercq, W., Agostinis, P., Vanden Berghe, T., Lippens, S., and Vandenabeele, P. (2010) Caspase-mediated cleavage of Beclin-1 inactivates Beclin-1-induced autophagy and enhances apoptosis by promoting the release of proapoptotic factors from mitochondria. *Cell Death Dis.* **1,** e18
99. Betin, V. M., and Lane, J. D. (2009) Caspase cleavage of Atg4D stimulates GABARAP-L1 processing and triggers mitochondrial targeting and apoptosis. *J. Cell Sci.* **122,** 2554–2566